Spring 2018

Computational Study of Lawesson's Reagent Mediated Fluorenone Dimerization Forming 9,9'-Bifluorenylidene

Andrew Jourdan Eckelmann
Missouri State University, Andrew080690@missouristate.edu

COMPUTATIONAL STUDY OF LAWESSON'S REAGENT MEDIATED FLUORENONE DIMERIZATION FORMING 9,9'-BIFLUORENYLIDENE

A Masters Thesis

Presented to

The Graduate College of

Missouri State University

In Partial Fulfillment

Of the Requirements for the Degree

Master of Science, Chemistry

By

Andrew Eckelmann

May 2018

COMPUTATIONAL STUDY OF LAWESSON'S REAGENT MEDIATED FLUORENONE DIMERIZATION FORMING 9,9'-BIFLUORENYLIDENE

Chemistry

Missouri State University, May 2018

Master of Science

Andrew Eckelmann

ABSTRACT

The ambition of this work is to start a path to the a priori rational design of high yield production for electron acceptors with finely tuned band gaps, from the comfort of an armchair. To this end, organic photovoltaics offer a cheap and sustainable means of manufacture using readily available materials and avoids the toxicity of some of the heavy metals used in first and second-generation solar cells such as cadmium. The microwave assisted Lawesson's reagent mediated one-pot one-step solventless synthesis takes less than 3 minutes and results in an 84% yield of 9,9'-bifluorenylidene from two equivalents of fluorenone. While fullerenes have traditionally been the most widely used electron acceptors in organic photovoltaics, bifluorenylidenes have been gaining attention due to their superior absorption in the visible spectrum, highly tunable band gap and cheap/efficient synthesis. Using an analog system to study the reaction divided into two parts; intermediate formation and sulfur extrusion, a molecular pathway has been devised that fits the reaction conditions and explains differences in % yields of substituted 9,9'-bifluorenylidenes reported in a manner readily conducive to making predictions based on the substituents chosen in the 9-fluorenylidene scaffold.

KEYWORDS: physical organic chemistry, computational chemistry, DFT, CASSCF, Lawesson's reagent, bifluorenylidene, organic photovoltaics, 1,2-dioxetane, 1,2-dithietane

This abstract is approved as to form and content

_____

Matthew R. Siebert, PhD.
Chairperson, Advisory Committee

COMPUTATIONAL STUDY OF LAWESSON'S REAGENT MEDIATED FLUORENONE DIMERIZATION FORMING 9,9'-BIFLUORENYLIDENE

By

Andrew Eckelmann

A Masters Thesis
Submitted to the Graduate College
Of Missouri State University
In Partial Fulfillment of the Requirements
For the Degree of Master of Science, Chemistry

May 2018

Approved:

_____
Matthew R. Siebert, PhD

_____
Gary A Meints, PhD

_____
Eric Bosch, PhD

_____
Ridwan Sakidja, PhD

_____
Julie Masterson, PhD: Dean, Graduate College

ACKNOWLEDGEMENTS

This work is a computational study of the wet lab synthesis of 9,9'-bifluorenylidene performed by Dr. Chad J. Stearman and Dr. Galen L. Eakins while at Missouri State University.

I dedicate this thesis to those who made it possible.

To all the friends I've made in my time here, far too many to list, I wish you all the best.

To Dr. Matthew R Siebert,

the best research advisor and mentor.

To my parents,

whom I owe my life,

without them I wouldn't exist.

TABLE OF CONTENTS

LIST OF TABLES

LIST OF FIGURES

CHAPTER 1: PHYSICAL-ORGANIC AND COMPUTATIONAL CHEMISTRY

Preamble

The Journal of Physical Organic Chemistry describes the field as a study of "the relationship between molecular structure and chemical reactivity in organic systems", "using results derived from experimental and computational methods."[1] While the experimental groundwork for the field began in the late 19th century and has continued to pick up since, it was not until 1940 that Louis P. Hammet coined the term "Physical Organic Chemistry" in an influential book by that same name.[2,3] Alongside this was the early development of computational chemistry building itself from a similar foundation of physical chemistry, growing over the years at an ever-increasing pace fueled by improvements in computational hardware.[4] However, it was not until 1998 when Walter Kohn and John Pople won a shared Nobel prize in chemistry for their work on density functional theory and computational methods in quantum chemistry that computational chemistry became universally recognized as its own fully distinct field.[5,6]

The following research project, upon which this thesis is written, requires an understanding of important concepts founded in both fields as well as upon prior experimental work.[7] This chapter will provide a foundation for understanding the research methodology employed and the interpretation of results on this computational study of a Lawesson's reagent mediated fluorenone dimerization forming 9,9'-bifluorenylidene.

Hückel Rules and Aromaticity

Benzene, first discovered by Michael Faraday in 1825, is among the most famous and widely recognized aromatic compounds and typically the first example presented in sophomore organic chemistry.[8] Historically, there is a strong connection between benzene and aromaticity because it was in 1855 that August Wilhem von Hoffman first used the term aromatic to refer to a list of "benzene like compounds" of which benzoic acid was the simplest.[9] Qualitatively, aromaticity is a cyclic delocalization of electrons that results in additional chemical stability than would otherwise be expected from π-bonded electrons.

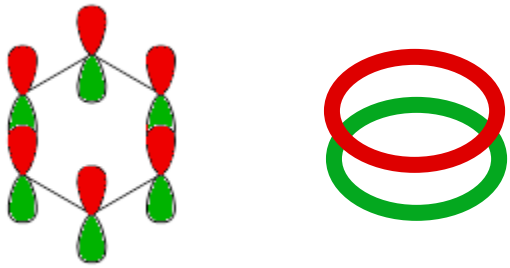

Localized p-orbitals Delocalized p-orbitals

Figure 1. Depiction of localized versus delocalized π-electrons in benzene.

It was Erich Hückel that first laid out the quantum mechanical foundation for the phenomenon in a series of publications.[10-12] William von Eggers Doering later articulated the modern expression "Hückel rules" by which it is typically first taught to students, $4n + 2$. [13] The Hückel rules for predicting the aromaticity of a molecule have four parts, the first stating that the number of π-electrons must be equal to $4n + 2$ such that n equals zero or is a positive integer. Second that those electrons be in a conjugated system. Third that the structure of the molecule be cyclic and fourth that the molecule be planar. Benzene

illustrates this well as a first example seeing that it has 6 π-electrons ($4n + 2 = 6$, where n=1). Additionally the system is conjugated with continuous *p*-orbitals in a cyclic and planar structure.

The modern view of aromaticity has expanded considerably to include more molecules than fit the traditional Hückel rules. [14] Molecules such as pyrene with 16 π-electrons across multiple fused rings have been shown to still be aromatic despite failing the $4n + 2$ rule (n=3.5). Furthermore, non-planar molecules such as fullerenes have also been shown to be aromatic despite not being flat so long as there is still sufficient orbital overlap to maintain a conjugated π-electron system.[15] The molecule of interest in this research project 9,9'-bifluorenylidene is also aromatic despite the fact that it does not precisely fit all the criteria for aromaticity in the Hückel rules.

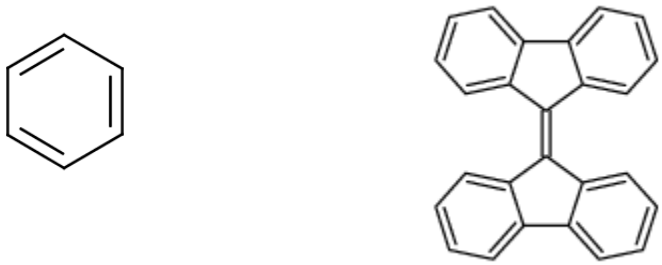

Figure 2. Bond line structure depiction of benzene and 9,9'-bifluorenylidene

9,9'-bifluorenylidene has 26 π-electrons ($4n + 2$, where n equals 6). Additionally, it has a continuous network of *p*-orbitals. However, it is not strictly speaking cyclic or planar (it is a bistricyclic aromatic ene) resulting in a dynamic cyclic delocalization of mobile electrons.[16] From this it has valuable applications as an electron acceptor in molecular electronics because upon accepting an electron it forms a stable radical making it an ideal

candidate for use as an *n*-type semiconductor in bulk heterojunction solar cells. Upon accepting an electron the π-bond connecting the two fluorene moieties breaks relieving the steric strain and the gain of an electron causes one side of the molecule to be an aromatically stabilized fluorenide anion that follows the classic Hückel rules with 14 π-electrons.[17]

Woodward-Hoffman Rules

Pericyclic reactions proceed through a concerted aromatic transition state.[18] Cycloaddition reactions are a subset of pericyclic reactions in which an equal number of π bonded electrons form an equal number of new σ bonds. To predict whether a cycloaddition reaction may proceed (that is if the reaction is deemed "forbidden" or "allowed"), Robert Burns-Woodward and Roald Hoffman developed rules to qualitatively predict relative barrier heights in pericyclic reactions known as the Woodward-Hoffman rules.[19] Development of these rules stems from conservation of orbital symmetry between reactants and products and predicts if a reaction will proceed thermally or photochemically.

To determine orbital symmetry a cycloaddition must be further specified with regard to orbital face and orientation of reactants using the terms suprafacial and antarafacial as seen in Figure 3 (next page). When the bonds formed in the cycloaddition are on the same face of the π system as are the termini of the π system involved in the bond formation the reaction is said to be suprafacial with respect to that reactant. If the opposite is true then it is termed antarafacial. Each reactant is then assigned a designation of suprafacial or antarafacial.

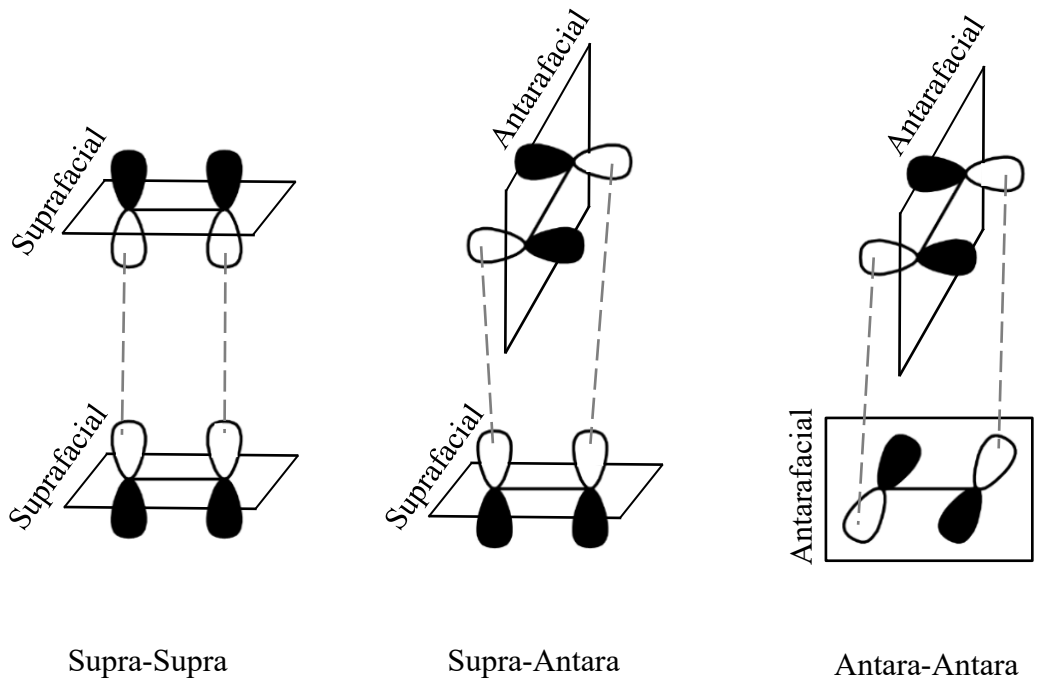

Figure 3. Depiction of all three possible combinations of suprafacial and antarafacial reactant orientations.

To illustrate this, consider the cycloaddition of two equivalents of ethylene to form cyclobutane. Because both reactants have two π bonded electrons the reaction is termed a [2+2] cycloaddition. Due to conservation of orbital symmetry, the symmetry of the orbitals in the reactants must match the symmetry of the orbitals in the product. In the case of a supra-supra orientation the symmetry elements preserved over the course of the reaction are two orthogonal planes defined as σ_1 and σ_2. Perpendicular to the *p*-orbital head to head interaction is σ_1 and perpendicular to the *p*-orbital side to side interaction is σ_2 as seen in Figure 4 (next page).

The four possible orbital phase combinations are then constructed starting with no nodes resulting in only constructive orbital overlap, building up to two nodes with no constructive overlap between the *p*-orbitals. Those four possible combinations of orbital

phases are ordered from lowest energy to highest energy as seen in Figure 5 (next page) where "*S"* stands for symmetric (resulting in constructive orbital overlap) and "*A"* stands for antisymmetric (resulting in deconstructive orbital overlap) with regard to *p*-orbital symmetry about σ_1 and σ_2.

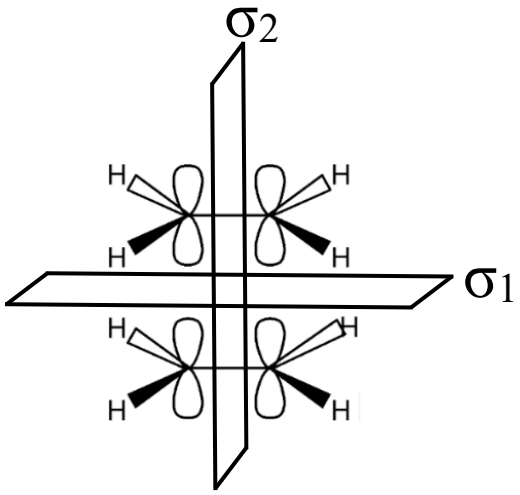

Figure 4. Depiction of two ethylene molecules such that σ_1 and σ_2 are orthogonal planes in which σ_1 is perpendicular to the p-orbital head to head interactions between the two ethylene molecules and σ_2 is perpendicular to the p-orbital side to side interactions within each ethylene molecule.

The single node orbital phase combination leading to a π^* interaction is higher in energy in the reactants than in the products whereas the single node orbital phase combination leading to a σ^* interaction is lower in energy in the reactants than in the products. The thermal pathway goes from the reactant in the ground state to the product in the excited state as depicted whereas the photochemical pathway goes from the reactants in an excited state to the product in the ground state. Due to the greater relative barrier height in the [2+2] thermal pathway it is deemed forbidden and the [2+2] photochemical pathway is deemed "allowed".

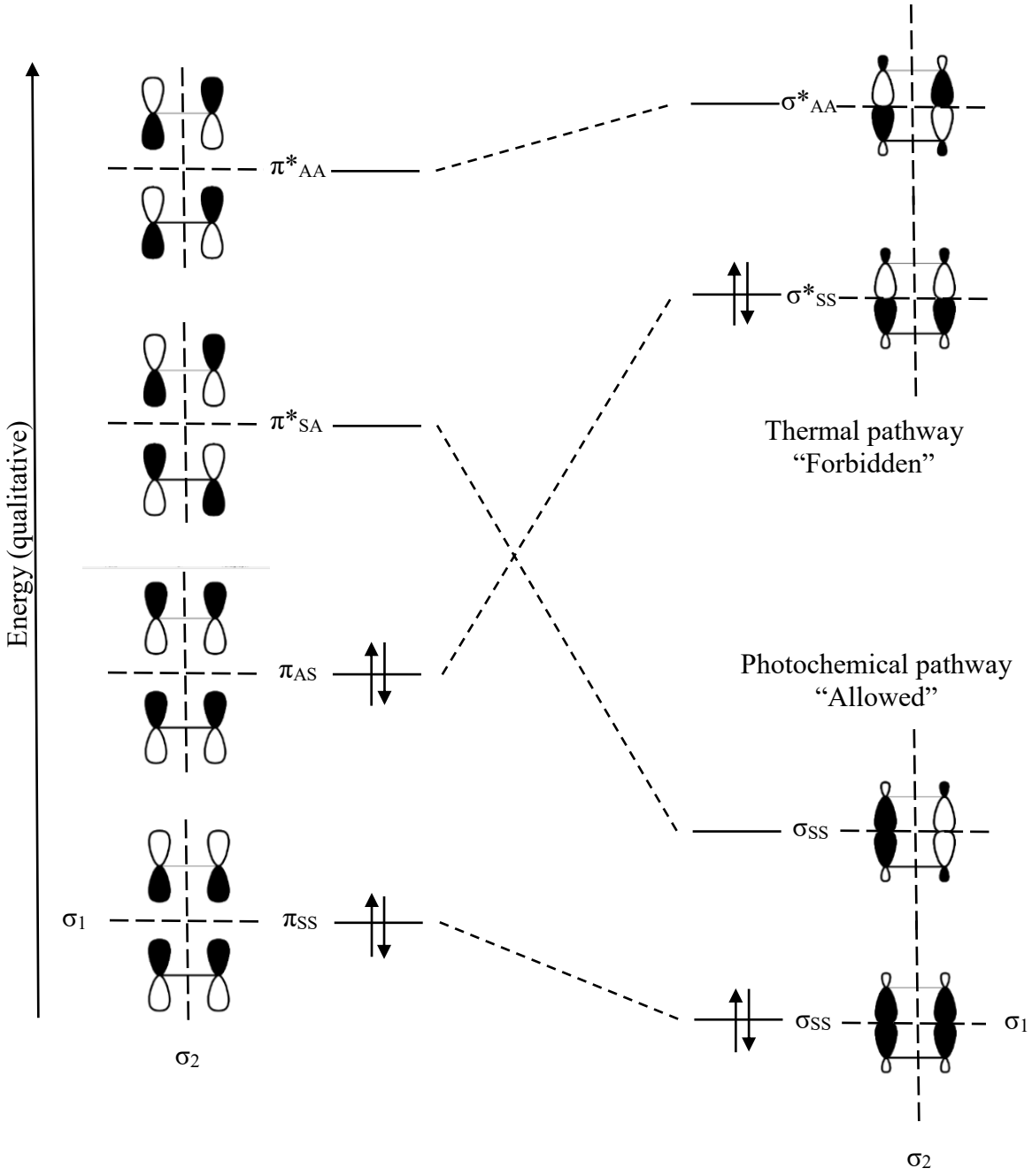

Figure 5. [2+2] Cycloaddition Woodward-Hoffman orbital correlation diagram of thermal and photochemical pathways for a supra-supra orientation.

If the orbital correlation diagram were constructed such that the symmetry elements preserved through the course of the reaction were for a supra-antara set of reactants then

the thermal reaction would be deemed “allowed” and the photochemical reaction “forbidden”.

Suprafacial/Antarafacial and Concerted Asynchronous Reactions

Cycloadditions are concerted reactions. A reaction is concerted when multiple bonds break and/or form within one transition state.[20] However, to be concerted does not mean that the multiple bonds have to break and form simultaneously within the one transition state. Concerted asynchronous reactions are a subclass of concerted reactions, in which a single transition state has multiple bond breaking and forming events that do not occur simultaneously.

To illustrate this consider the example of two equivalents of ethylene forming cyclobutane in a [2+2] cycloaddition reaction. The allowed pathways are supra-supra orientation for photochemical and supra-antara orientation for thermal as depicted below in Figure 6.[18]

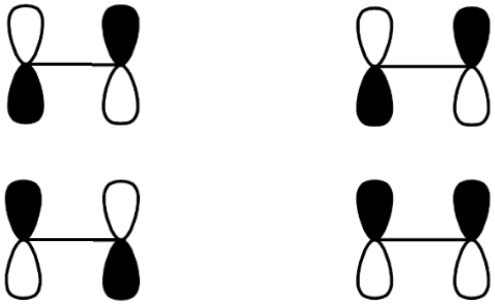

Figure 6. Depiction of the [2+2] cycloaddition reactant orientations for a photochemical supra-supra pathway and a thermal supra-antara pathway.

The supra-supra photochemical reaction pathway already has the *p*-orbital phases oriented facing each other, such that constructive overlap between the *p*-orbitals of the two π-systems yielding the two new σ-bonds occurs simultaneously, in concerted fashion.

Whereas the supra-antara thermal reaction pathway has only one *p*-orbital of either π-system oriented for constructive overlap, yet, still also proceeds in a concerted fashion. In the thermal pathway as the first bond forms suprafacially the *p*-orbital of the second rotates to present its backside (antarafacially). Because of the conformational adjustment the formation of the first and second bond do not occur simultaneously but they do both form within the same transition state. Thus, the supra-antara thermal pathway is an example of a concerted asynchronous reaction.

Empirical analog: Dioxetane Thermal Decomposition

An important chemical scenario to consider in understanding the mechanism of fluorenone dimerization to 9,9'-bifluorenylidene is the empirically observed thermal decomposition of 1,2-dioxetane systems resulting in a high yield of excited state products. It's process of decomposition may hold clues to the formation of intermediates preceding sulfur extrusion in the formation of 9,9'-bifluorenylidene. As such, 1,2-dioxetane is used as one of five intermediate analog systems investigated in this thesis.

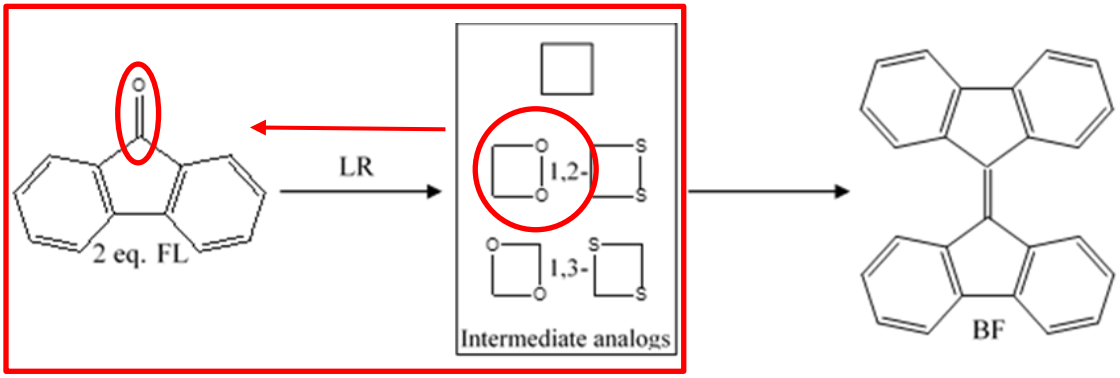

Figure 7. Experimental scheme to model the synthesis of 9,9'-bifluorenylidene. The red box highlights the analogous portion to the thermal decomposition of 1,2-dioxetane systems. The red arrow indicates the empirically observed thermal decomposition.

The thermal decomposition of 1,2-dioxetane systems to excited state products was first reported by Kopecky and Mumford in 1968 after observing luminescence in 3,3,4-trimethyl-1,2-dioxetane when heated to 60 °C.[21] Collectively, they represent the largest class of isolable molecules forming high yields of products in an excited state from an uncatalyzed thermal decomposition.[22] The simplest conceivable system of which would yield two equivalents of formaldehyde along with an emission of light. In the process of thermal decomposition two equivalents of formaldehyde are produced asymmetrically in excited singlet and triplet states accounting for the fluorescence and phosphorescence.[23] The proposed mechanisms in the literature representing possible pathways explaining the thermal dissociation of 1,2-dioxetane systems are either: biradical involving two transition states; or concerted, broken into synchronous and merged (asynchronous) mechanisms as seen below in Figure 8.[24-27]

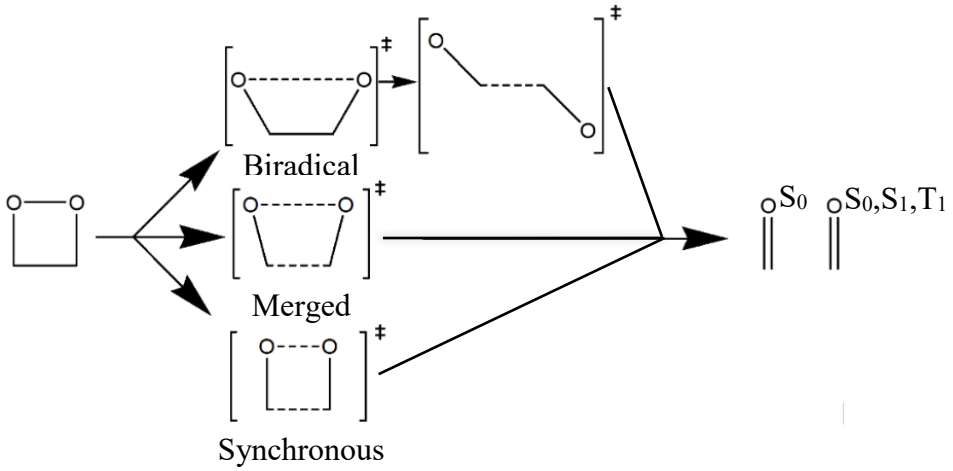

Figure 8. Depiction of three proposed pathways for the thermal decomposition of 1,2-dioxetane to two equivalents of formaldehyde. Products are generated in the ground state as well as singlet and triplet excited states.

To understand how the products are formed in excited states it is prudent to first explore some fundamentals of quantum mechanics that will also lay the foundation of the computational methods used in this chemical investigation.

Schrödinger Equation and the Born-Oppenheimer approximation

At the heart of computational chemistry is the Schrödinger equation named after Erwin Schrödinger who derived it in 1925 and published it in 1926.[28] It exists in two general forms depending on if it is time-dependent or time-independent. The time-independent Schrödinger equation is an eigenvalue equation and the wave function is an eigenfunction of the Hamiltonian operator in which the wave function contains all of the information regarding the quantum mechanical system of interest.

$$\widehat{H}\Psi = E\Psi$$

Equation 1. Time-independent Schrodinger equation. $\widehat{H}$, is the Hamiltonian operator. Ψ is the wave function describing the system. E is the systems energy.

That is, the Hamiltonian operator acts on a wave function and if the result is proportional to the original wave function then that original wave function is a stationary state and the proportionality constant E is the total energy of the system. It can be thought of in qualitative terms as analogous to querying an oracle.[29] Where the Hamiltonian operator is the oracle, the wavefunction is the question and the energy is the answer.

The calculated total energy of the system is composed of kinetic and potential energy from interactions of the electrons and nuclei comprising the system.

$$\hat{H} = Total\ Energy$$

$$\hat{H} = T + V$$

$$\hat{H} = T_e + T_n + V_{en} + V_{ee} + V_{nn}$$

Equation 2. Hamiltonian operator broken into specific energy terms. T is kinetic energy, V is potential energy, T_e is kinetic electron energy, T_n is nuclear kinetic energy, V_{en} is electron-nuclear potential energy, V_{ee} is electron-electron potential energy, V_{nn} is nuclear-nuclear potential energy.

This results in five separate terms. Two for the kinetic energy, one each for the electrons (T_e) and one for nuclei (T_n). Then three for the potential energy, electron-nucleus (V_{en}), electron-electron (V_{ee}) and nucleus-nucleus (V_{nn}). All terms are negative except for potential energy from electron-electron and nucleus-nucleus interactions as they are of like charge and result in repulsion raising the energy of the system.

$$\hat{H} = -\sum_i \frac{\hbar^2}{2m_e}\nabla_i^2 - \sum_k \frac{\hbar^2}{2m_k}\nabla_i^2 - \sum_i \sum_k \frac{e^2 Z_k}{r_{ik}} + \sum_{i<j} \frac{e^2}{r_{ij}} + \sum_{k<l} \frac{e^2 Z_k Z_l}{r_{kl}}$$

Equation 3. Hamiltonian operator break down of specific energy terms. *i* and *j* are electrons, *k* and *l* are nuclei, ħ is Planck's constant divided by 2π, ∇^2 is the laplacian operator, m_e is electron mass, m_k is nuclear mass, *e* is electron charge, *r* is distance separating particles, Z is atomic number.

In order to simplify solving for the system's energy, a key approximation known as the Born-Oppenheimer approximation is employed. This allows chemists for a fixed set of nuclear coordinates to replace nuclear repulsion with a constant and eliminate nuclear kinetic energy.[30] This is rationalized on the basis that an electron is approximately 1800 times lighter than a hydrogen nucleus and as such an electron responds to any change in nuclear coordinates near instantaneously. The profound

implication of this is the ability to generate a potential energy surface for any fixed nuclear coordinate.

Potential Energy Surface

The concept of the potential energy surface helps us explain important concepts in chemistry such as equilibria and kinetics.[31] Specific landmark points on a potential energy surface correspond to key points within a reaction coordinate diagram regarding a molecule's structural transformations such as conformational changes or bonds breaking and forming. It is a representation of a molecule's energy graphed against its three-dimensional geometry producing a hyper surface. This means that an *n*-atom molecule can be described by an *N*-dimensional adiabatic potential energy surface for which every *N* dimensions are comprised of 3*n*-6 nuclear geometry coordinates and one energy coordinate. To help visualize this consider that each structure has a unique energy and changes in the geometry of that structure is a smooth process, so, too the corresponding change in energy creates a smooth energy landscape. This view of the potential energy surface can be thought of as making chemistry into topology as seen in Figure 9.

Local minima on this surface from which energy increases for all three Cartesian coordinates corresponds to energy minima within a reaction coordinate diagram. These energy minima being the reactants, products and stable intermediates that exist within a chemical reaction. Transition states connect these energy minimum structures, with the structure of the transition state lying between the two structures of the corresponding minima most closely resembling the minimum, which it is closest to in energy.[32] On the potential energy surface, transition states are located on saddle points in which a local

minimum is perpendicular to a local maximum. Following along in the two directions in which the energy decreases then connects the transition state structure to its corresponding energy-minimum structures.

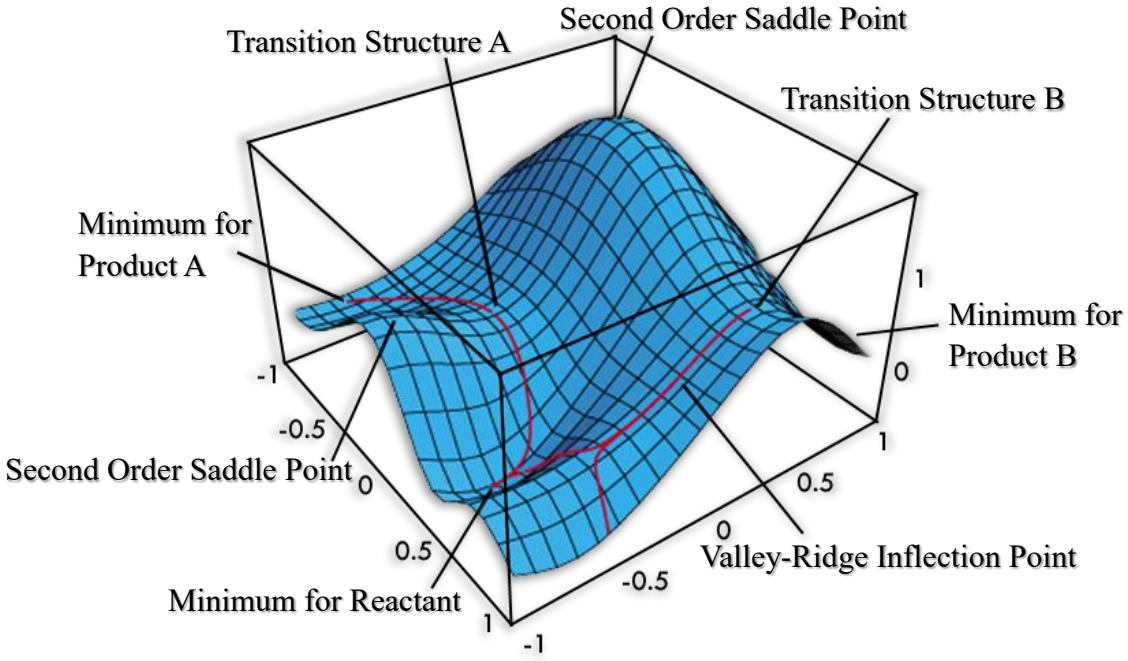

Figure 9. Depiction of a hypothetical potential energy surface.[29] The red line illustrates pathways connecting landmark points on the potential energy surface for reactants and products seen at energy minima as well as the transition states between minima located at saddle points on the surface. A valley ridge inflection point occurs when one transition state leads to multiple products. Second order saddle points correspond to chemically non-meaningful transitions states.

For every possible electronic configuration for a given molecule there exists a potential energy surface specific to that electronic configuration of that molecule, such that there are *n* potential energy surfaces for *n* electronic configurations.[29] The Born-Oppenheimer approximation holds well so long as the electronic configurations are well-separated in energy. However, when a specific nuclear coordinate geometry has two electronic configurations that are degenerate it results in a conical intersection as seen in

Figure 10 between the two potential energy surfaces. At this point the electrons may crossover from one configuration to the other, resulting in a breakdown of the Born-Oppenheimer approximation. The conical intersection is so named because when plotted in subspace using orthogonal axes of potential energy, gradient difference and differential coupling the topology of the intersection takes on the shape of two cones connected at their points.[22] Their primary axis is parallel to potential energy and perpendicular to gradient difference and differential coupling. The upper cone in Figure 10 represents a "funnel" on the excited-state surface allowing a high efficiency path by which a higher energy electronic state can relax to a lower energy state.

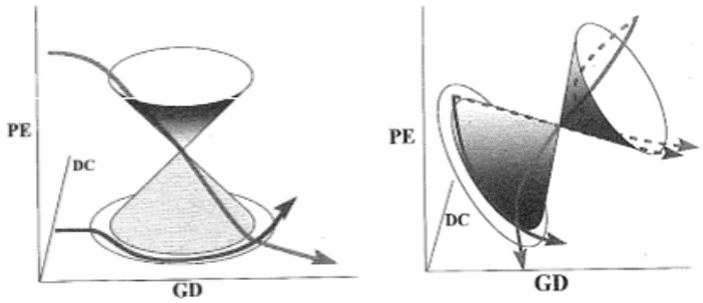

Figure 10.[22] Conical Intersection of Two Potential Energy Surfaces. PE is potential energy, GD is gradient difference and DC is derivative coupling. Adapted from Carpenter, B. K. Electronically nonadiabatic thermal reactions of organic molecules.

Molecules reacting on the ground-state surface bypass the lower cone in an avoided crossing. There are situations however, in which the conical intersection is tilted resulting in reactants forming products in their excited state as seen on the right of Figure 10.[22] An example is the previously mentioned thermal decomposition of 1,2-dioxetane systems resulting in the formation of excited singlet and triplet state products responsible for the fluorescence and phosphorescence first observed by Kopecky and Mumford.[21] Multistate multiconfigurational second-order perturbation theory has been used to

rationalize the chemiluminescence as a result of entropic trapping between triplet and singlet potential energy surfaces occurring after the O-O cleavage of 1,2-dioxetane in agreement both qualitatively and quantitatively with empirical studies.[33] Figure 11 depicts the intersecting singlet and triplet potential energy surfaces during the thermal dissociation.

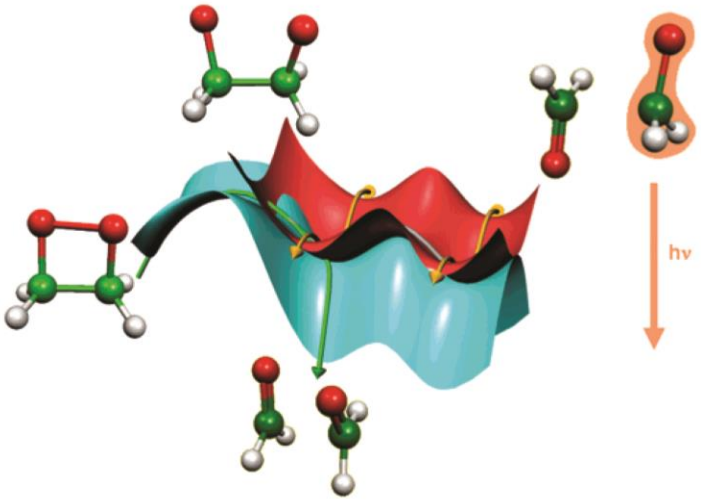

Figure 11.[33] Depiction of the intersecting singlet and triplet potential energy surfaces responsible for excited state formation in the thermal dissociation of 1,2-dioxetane. The primary reaction coordinate is torsion about the O-C-C-O dihedral. Perpendicular to that is distance between the C-C bond and running vertically is the energy of the system. Adapted from De Vico, L.; Liu, Y. J.; Krogh, J. W.; Lindh, R. Chemiluminescence of 1,2-Dioxetane. Reaction Mechanism Uncovered.

The primary reaction coordinate is torsion about the O-C-C-O dihedral. Perpendicular to that is the distance between the C-C bond and running vertically is the energy of the system. The conical intersection runs along the seams at which the two potential energy surfaces are degenerate in energy.

CHAPTER 2: MOLECULAR ELECTRONICS AND PHOTOVOLTAICS

History and Future

The first generation of modern solar cells were made from crystalline silicon, the second generation made use of amorphous silicon among other new materials such as cadmium telluride.[34,35] The newest third generation of solar panels has expanded in scope considerably with various organic photovoltaics (solar inks, dyes, conductive plastics and new doping agents) offering an additional means to improve upon the efficiency/cost-effectiveness of current solar panel technologies meanwhile furthering the environmental sustainability afforded by solar power. Organic photovoltaics are produced from readily available materials and avoid the toxicity associated with heavy metals (e.g., cadmium) making them cheaper and safer to manufacture.

Presently, most organic photovoltaic *n*-type semiconductors used in bulk-heterojunction solar cells are fullerene derivatives that are marred by weak absorption in the visible spectrum and are difficult to synthesize/purify.[36] Bifluorenylidenes show great promise as an alternative *n*-type semiconducting material as they will readily accept an electron forming a stable radical and exhibit strong absorption in the visible region due to a highly tunable HOMO-LUMO band gap.[16,37] Additionally, there exists a very quick, simple and efficient solvent-less one-pot one-step synthesis.[7]

Insulator, Conductor, Semiconductor

A consequence of orbital conservation is that when molecular orbitals are derived from multiple atoms every interacting pair of atomic orbitals forms two molecular

orbitals (bonding and antibonding).[38] Thus it follows that *n* atomic orbitals produce *n* molecular orbitals and because in bulk solids the number of atoms is very large, so too will the number of orbitals be very large. The close spacing of energy levels between orbitals for this large number of atoms results in bands of orbitals as opposed to the discrete energy levels encountered with individual small molecules. The highest energy band containing electrons is termed the valence band followed by the next highest energy band termed the conduction band. The separation in energy between these two bands forms the classification for conductors, semiconductors and insulators.

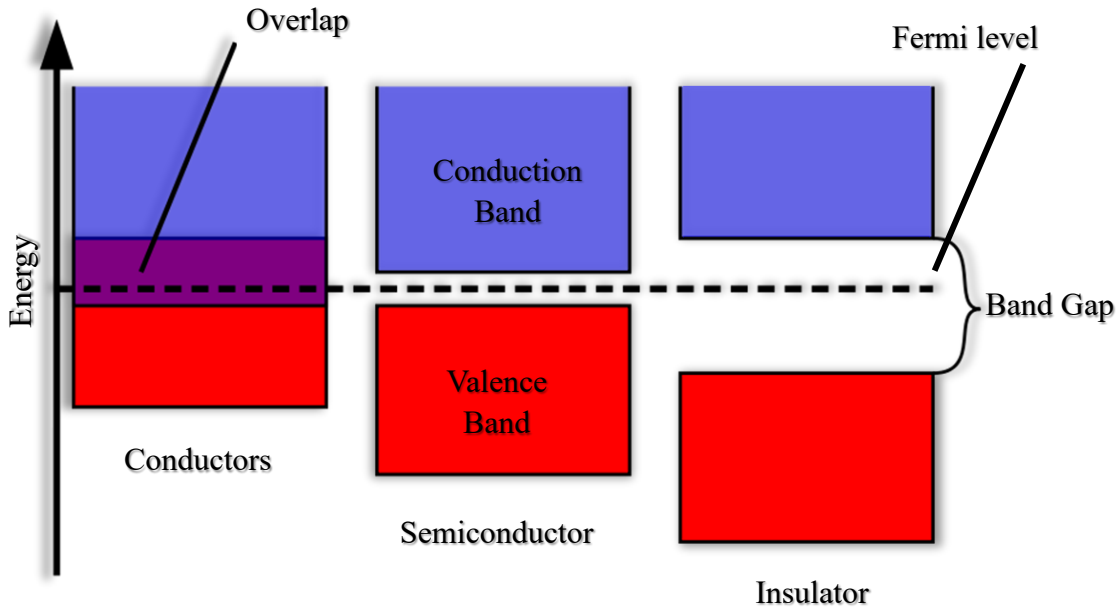

Figure 12. Depiction of the relative energy for the conduction band and valence band in conductors, semiconductors and insulators. The Fermi level is the energy at which an electron is equally likely to be in the valence band or conduction band.

Conductors allow electrons to easily move from one band to the other due to overlap between the valence and conduction band. Semiconductors have a band gap that allows electrons to move from valence to conduction band given sufficient energy. The band gap for insulators is large such that the energy required for an electron to move from

valence band to conduction band is relatively insurmountable.

When an electron is excited, moving from the valence band to conduction band, it creates an electron hole pair with the electron now in the conduction band and a resultant electron hole in the valence band. Semiconductors can be doped to increase or decrease their conductance under applied voltage as either an *n*-type (negative) or *p*-type (positive) semiconductor depending on the properties of the dopant relative to the host material. If the dopant has more electrons in the valence shell than the host material it promotes electrons from the dopant to move from the valence band into the conduction band of the host material (*n*-type semiconductor). Whereas if the dopant has fewer electrons in the valence shell than the host material it creates positive holes promoting electrons from the host to move from the valence band to the conduction band of the dopant (*p*-type semi-conductor).

The Fermi level then predicts the energy at which an electron is equally likely to be in either the valence band or conduction band, which depends on temperature and the energy of the band gap. In an *n*-type semiconductor the fermi level is raised and in a *p*-type semiconductor the fermi level is lowered. Layering *n*-type and *p*-type semiconducting materials along with insulators is then the foundation of designing integrated circuits in the modern electronics industry in which controlling an applied voltage at junctions between layers determines conductance.

Photovoltaic Effect / Photovoltaic Cells

When *p*-type and *n*-type semiconductors are layered, the region where they meet is termed a *p*-*n* junction.[38,39] At the point of contact an equilibrium is quickly established

as electrons flow from the *n*-type semiconductor to fill holes in the valence band of the *p*-type semiconductor. As electrostatic forces increase, the flow of electrons slows resulting in a negative charge on the *p*-type side of the junction and a positive charge on the *n*-type side. This separation of charge halts any additional electron flow across the junction and brings the fermi level of both sides to be equal in energy.

Photons of sufficient energy may then promote electrons from the valence band of the *p*-type side to the conduction band of the *n*-type side resulting in a photinduced charge. With external connections made to both sides of the *p*-*n* junction a current is established as long as photons of sufficient energy continue to be absorbed by the *p*-*n* junction.

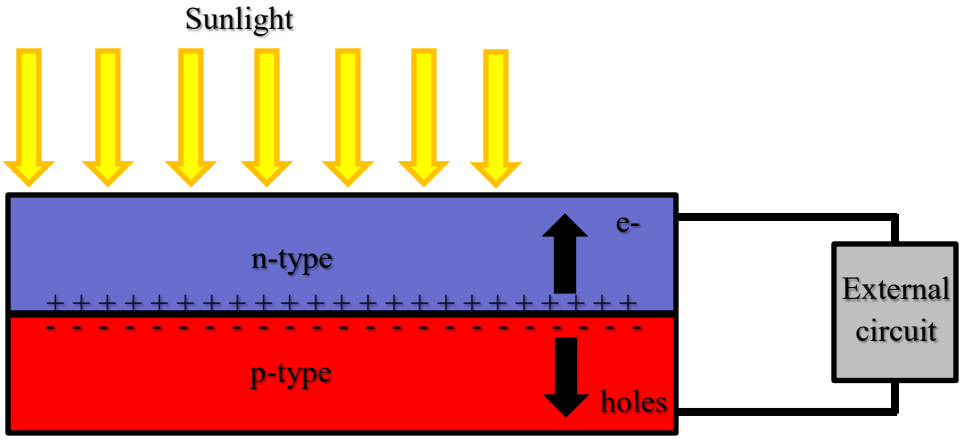

Figure 13. Schematic of a solar cell. Charge builds up at the *p*-*n* junction and then a current is established driven by a photo-induced charge from absorption of photons promoting electrons from the valence band of the *p*-type side to the conduction band of the *n*-type side.

This current can then be fed through an external circuit to charge a battery, power a light bulb or feed into the power grid. This phenomenon played in reverse forms the foundation of light emitting diodes.

Band Gap Tuning in Solar Cells

The active layer of the solar cell is the bulk heterojunction and functions by photo-induced charge transfer between a donor-acceptor pair.[39] In an organic photovoltaic cell charge transfer occurs between the electron donating material (a *p*-type semiconductor), such as a light absorbing and hole conducting polymer in to the electron accepting component (an *n*-type semiconductor), most commonly a fullerene or one of its derivatives. When picking a donor acceptor pair it is necessary to consider the energy levels of the highest occupied molecular orbital (HOMO) and the lowest unoccupied molecular orbital (LUMO) because the difference in energy between donor and acceptor must be complimentary for charge transfer to occur.[40] Currently, there is a large list of diverse new polymeric donor structures capable of absorbing light over a wide range of wavelengths and have a small energy gap facilitating charge transport such as polyacetylene, poly-*p*-phenylene, poly-*p*-phenylenevinylene, oligothiophene, polythiophene, polythienylenenvinylene, polypyrole and polyfluorene.[41,42] However, outside of fullerene and it's derivatives there have been comparatively far fewer new organic electron accepting materials proposed in the literature.

Bifluorenylidenes present a promising alternative to fullerene. They are more easily synthesized in large quantities. They have a highly tunable HOMO-LUMO band gap more compatible with most available electron donating organic materials due to a change in aromaticity when accepting an electron. Additionally, there is a large wealth of possible substituent modifications that can be made to their base structure to further tune their HOMO-LUMO band gap.[43]

CHAPTER 3: BIFLUORENYLIDENE

Bistricyclic Aromatic Enes

9,9'-bifluorenylidene falls into a larger category of molecules known as bistricyclic aromatic enes (BAEs) that follow the general structure shown in Figure14.[44] Furthermore, BAEs can be subcategorized as either homomerous or heteromerous depending on if the molecule is symmetric about the fjord or not. Another way to put it is if X=Y then the BAE is homomerous and if X≠Y the BAE is heteromerous.

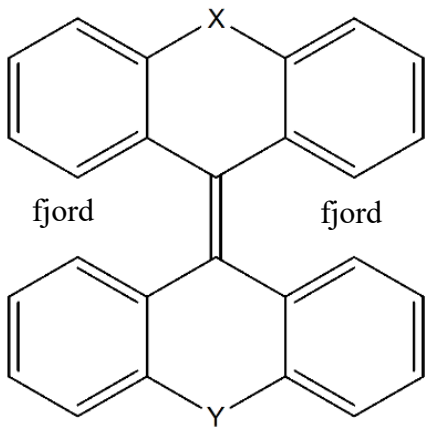

Figure 14. Schematic of a generic bistricyclic aromatic ene. X and Y can be any atom or combination of atoms including no atoms such as is the case with 9,9'-bifluorenylidene.

Molecules with this general structure are known for dynamic stereochemistry and switchable spectroscopic properties including thermochromism and photochromism. This is owed to an interplay between the stability conferred by aromaticity and a steric repulsion between substituents in the fjord regions resulting in deviation from the ideal planarity of an aromatic system. The structure of 9,9'-bifluorenylidene seen in Figure 15 consists of two fluorene moieties bonded at the 9 and 9' positions and the fjords are between positions 8,1' and 1,8'.

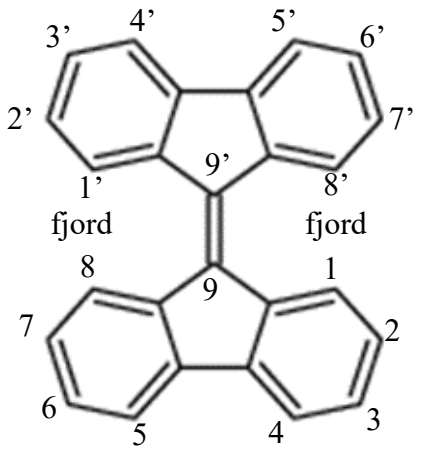

Figure 15. Depiction of 9,9’-bifluorenylidene illustrating the bistricyclic aromatic ene substituent numbering scheme.

9,9’ bifluorenylidene is the smallest of the bistricyclic aromatic enes and as a result of which it is the least sterically encumbered. This gives it a stronger proclivity towards planarity than other BAEs but does not give it the planar structure that the sp^2 hybridization its 9 and 9’ carbons would suggest. With just hydrogen atoms, the smallest possible substituents in the fjord region 9,9’-bifluorenylidene still has a dihedral angle between the two fluorene moieties of 32°.[45] If the substituents in the fjord region are changed to fluorine atoms the dihedral twist results in an angle of 40.3° and larger chlorine atoms likewise further increase the dihedral to 52.6°.[46]

Tunable Band Gap

Adding substituents to 9,9’-bifluorenylidene and modulating the dihedral angle provides a great tool by which to tune the HOMO-LUMO band gap.[37] Without modification the native bandgap is 2.47 eV. As the dihedral angle increases so, too, does the band gap. As the constructive overlap between the *p*-orbitals of the 9 and 9’ carbons

decreases this effectively reduces conjugation between the two fluorene moieties increasing the energy of the LUMO and decreasing the energy of the HOMO.

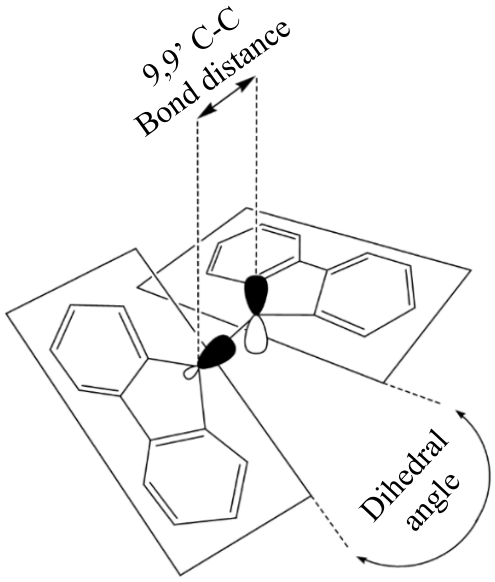

Figure 16. Depiction of the torsional strain from steric repulsion between substituents at the 1,8 and 1',8' positions. The *p*-orbitals illustrate the reduced conjugation as the planes of the two flourene moieties twist away from one another reducing the side to side π interaction.

Adding substituents has a smaller and mixed effect on the band gap, depending on if the substituent is electron-withdrawing or -donating. Electron-donating substituents increase both the HOMO and LUMO but increase the HOMO more than they increase the LUMO resulting in a net decrease in the band gap, while the reverse is true for electron-withdrawing substituents. Halogens produce a mixed effect as the trends of size and electronegativity run against one another moving up and down the periodic table. Fluorine being smaller and more electronegative than chlorine results in an increase in the band gap while chlorine substituents create a decrease in the band gap.

Synthesis / Possible Mechanism

9,9'-bifluorenylidene was first synthesized in 1875. [47] Since then several additional novel methods have been proposed in the literature.[48] The synthetic scheme of interest in this thesis is a solvent-less one-pot one-step green synthesis performed by Dr. Galen Eakins while a graduate student at Missouri State University in Dr. Chad Stearman's research group.[7] The only two reactants are fluorenone and Lawesson's reagent, finely ground and mixed together in a 2:1 molar ratio. This reactant mixture then undergoes microwave assisted synthesis for 162 seconds reaching a maximum temperature of 152°C. The formed product is then dissolved in minimal toluene and purified by column chromatography resulting in an 84% yield.

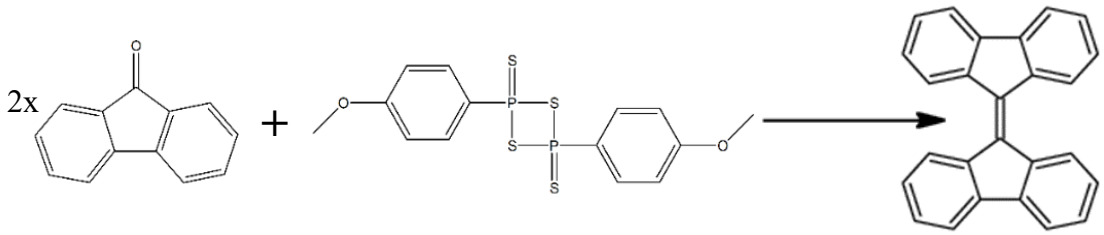

Figure 17. Reactants and products of the 9,9'-bifluorenylidene synthesis performed by Dr. Galen Eakins while a graduate student at Missouri State University in Dr. Chad Stearman's research group. Fluorenone and Lawesson's reagent are mixed together in a 2:1 ratio.

Lawessons's reagent is a chemical species first synthesized in 1956 by Lecher et al,[49] but gets its name from Sven-Olov Lawesson who popularized it through extensive experimentation examining its reaction with a large list of different functional groups.[50] Lawesson determined that it reacted with carbonyl containing functional groups

proceeding through an oxathiophosphetane ring ultimately yielding a thionated carbon as seen in Figure 18 with the example fluorenone.

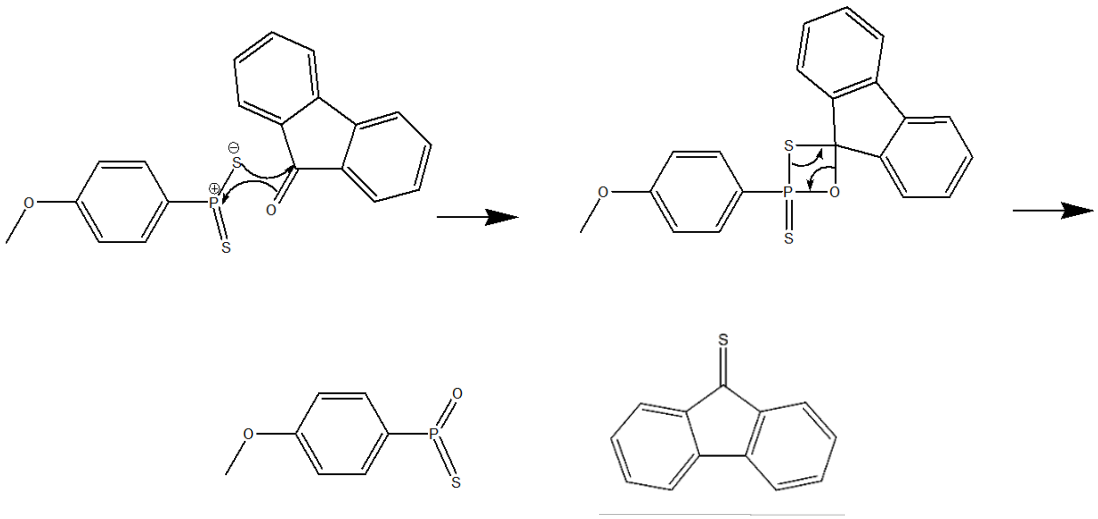

Figure 18. Arrow pushing thionation of fluorenone by Lawesson's reagent.

It is not known how the thionated fluorenone species dimerize to form bifluorenylidene. This study follows Occam's razor and investigates the possibility of 1,2- and 1,3-intermediate structures leading to formation of 9,9'-bifluorenylidene as seen in Figure 19 below.

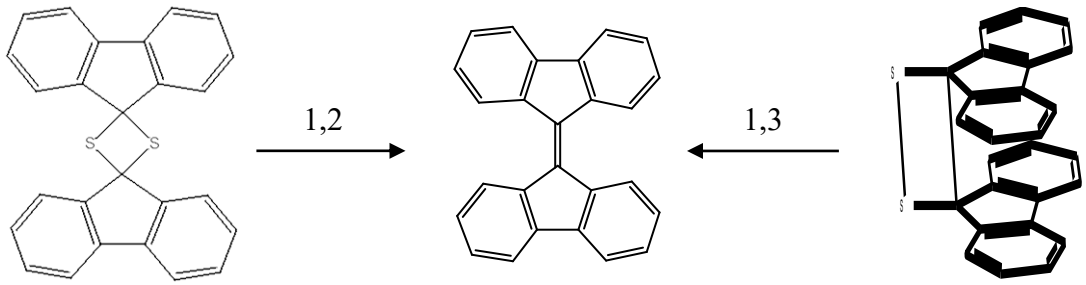

Figure 19. Depiction of possible 1,2- and 1,3-intermediates leading to the formation of 9,9'-bifluorenylidene.

CHAPTER 4: EXPERIMENTAL AND COMPUTATIONAL METHODS

Computational Chemistry Software

In performing computational chemistry research scientists make use of computer software to interface with computer hardware that run calculations and extract pertinent information describing chemical systems. The following is a general overview of the computational research process for this body of work. Molecules are first constructed in GaussView 6 and subsequent calculations performed with Gaussian 16. Jobs are created and submitted to an in-house computational cluster lovingly named Grizzly using PuTTY. Then WinSCP is used to transfer files between a remote computer (in our case Grizzly) and the local computer. Excel is finally used to organize and manage jobs already ran and assist in analysis of important information extracted from the completed calculations.

GaussView 6 is the most recent edition of the graphical user interface associated with Gaussian.[51] It allows for the construction and visualization of molecules. Output results from completed jobs can also be visualized using GaussView 6 such as molecular orbitals or animating vibrations. Gaussian 16 is the most recent edition in the suite of Gaussian programs utilized by scientists and engineers both in industry and academia.[52] The first edition named Gaussian 70 was released by noble laureate John Pople in 1970, originally created as a collaboration with his research group at Carnegie Mellon University. [57] However, since 1987 it has been developed and licensed by a private company, Gaussian Inc. Today it offers electronic structure modeling for a diverse and large number of computational methods.

Instead of using GaussView 6 to setup and submit jobs we use PuTTY, a free open-source SSH and telnet client application. It is operated by command line interface rather than a graphical user interface. When creating a job, the model chemistry is specified by functional and basis set along with any additional keywords to instruct the calculation. The chemical system itself is specified by spin multiplicity, charge and atomic geometry either in Cartesian coordinates or z-matrix.

Computational Chemistry Theory

The field of computational chemistry itself grew out of quantum chemistry as a means for solving the Schrödinger equation.[29] Douglas Hartree's self-consistent field theory (SCF) marks one of the early major landmarks of computational chemistry, first proposed in 1927 only 1 year after the publication of the Schrödinger equation. Self-consistent field theory offers an iterative method for solving the Schrödinger equation starting with an initial guess wave function (representing a set of atomic or molecular orbital). The variational principle can be used to modify the approximate wave function closing in on the optimal wave function. The Hartree-Fock method came about later in which Vladimir Fock introduced Slater determinantal wave functions as the trial wave functions. This was done in order to satisfy the Pauli Exclusion Principle stemming from the antisymmetry inherent to a wave function with respect to the exchange of two electrons. As a general property of a determinant when any two columns or rows are interchanged so too does the sign of the determinant flip mirroring the spin restrictions on two electrons sharing an orbital. Equation 4 below illustrates a Slater determinant used

for creating an antisymmetric wave function suitable for describing atomic and molecular orbitals.

$$\Psi_{SD} = \frac{1}{\sqrt{N!}} \begin{bmatrix} \chi_1(1) & \cdots & \chi_N(1) \\ \vdots & \ddots & \vdots \\ \chi_1(N) & \cdots & \chi_N(N) \end{bmatrix}$$

$$\Psi_{SD} = |\chi_1 \chi_2 \chi_3 \cdots \chi_N\rangle$$

Equation 4. Slater determinant. χ represents the spin-orbital (product of a spatial orbital and an electron spin eigenfunction). *N* is the total number of electrons.

In order to solve the time-independent Schrödinger equation for any system more complex than a hydrogen atom approximations must be put in place, otherwise the problem becomes intractable.[31] In chapter 1 (pages 11-12) we already discussed the Born-Oppenheimer approximation in which the time-independent Schrödinger equation is simplified by reducing the nuclear-nuclear repulsion energy to a constant and nuclear kinetic energy. This approximation allows for the calculation of electronic energy from a static set of nuclear coordinates. Equation 5 below shows the electronic derivation of the Schrödinger equation for a single electron system after invoking the Born-Oppenheimer approximation where the orbitals are represented by the eigenfunctions of the equation.

$$\left(\widetilde{H} + V_N\right) \Psi(q_i; q_k) = \tilde{E}\, \Psi(q_i; q_k)$$

Equation 5. Single electron system, electronic derivation of the Schrödinger equation. $\widetilde{H}$ is the electronic Hamiltonian. $\tilde{E}$ is the electronic energy. Ψ is the wave-function. V_N is nuclear repulsion energy. q_i is the independent electronic coordinates and q_k is the nuclear coordinates.

This is carried into the Hartree-Fock method with a similar additional approximation to handle the electron-electron interactions for a many electron wave-function because electron correlation for a many body system still represents an intractable problem.[29] Hartree-Fock views each system as a set of singly occupied molecular orbitals as a means of side stepping electron-electron correlation. Making an *N*-electron problem into an *N* single-electron problem. In place of electron correlation, a mean-field approximation is employed allowing individual electrons to move independently in an averaged field of charge generated by all the electrons in the system. This external charge is represented by Equation 6, the Hartree-Fock potential.

$$V_i\{j\} = \sum_{j \neq i} \int \frac{\rho_j}{r_{ij}} dr$$

Equation 6. Breakdown of the Hartree-Fock potential. $V_i\{j\}$ is the Hartree-Fock potential and represents the interaction potential from all other electrons *i* in orbitals $\{j\}$. ρ_j is charge density. r_{ij} is distance between electrons.

Replacing electron-electron correlation by the external charge (Hartree-Fock potential) now gives us the Hartree Hamiltonian seen below in equation 7.

$$\tilde{h} = -\frac{1}{2}\nabla_i^2 - \sum_{K=1}^{M} \frac{Z_k}{r_{ik}} + V_i\{j\}$$

Equation 7. Breakdown of the Hartree Hamiltonian. $\tilde{h}$ is the Hartree Hamiltonian. ∇^2 is the laplacian operator. Z is the atomic number of the nucleus. r_{ik} is the distance between the electron and nucleus. $V_i\{j\}$ is the Hartree-Fock potential.

The time-independent Schrödinger equation allows us to solve for the orbitals of a hydrogen atom exactly.[28,31] For the purposes of computation, these atomic orbitals are

built from a basis set composed of Gaussian functions, hence the name of the computational program Gaussian.[29,52,53] When describing a model chemistry, the basis set is the collection of the Gaussian basis functions used in building those atomic orbitals. From these atomic orbitals we form a wave function representing molecular orbitals by linear combination of atomic orbitals as seen below in Equation 8.

$$\Phi_i = \sum_n C_{ni}\varphi_n$$

Equation 8. Linear combination of atomic orbitals (LCAO) for constructing molecular orbitals. $\Phi_i$is the molecular wavefunction. *C* is a coefficient weighting the contribution of each atomic orbital. φ_n is the nth atomic orbital.

Combining the molecular wave function from equation 8 and the Hartree Hamiltonian of equation 7 yields the new Hartree modified Schrödinger equation as shown in equation 9.

$$\widetilde{h_\iota}\Phi_i = E_i\Phi_i$$

Equation 9. Hartree modified Schrödinger equation. $\widetilde{h_\iota}$ is the Hartree Hamiltonian. Φ_i is the molecular wave function. E_i is the electronic energy.

Now armed with the Hartree modified Schrödinger equation we are able to tackle the SCF cycle. The crux of which is the variational principle of quantum mechanics. As seen below in Equation 10.[31]

$$E = \langle E \rangle = \frac{\int \Psi^* \widehat{H} \Psi \, dr}{\int \Psi^* \Psi \, dr} \geq E^{exact}$$

Equation 10. Variational principle of quantum mechanics. *E* is the energy of the system. $\widehat{H}$ is the Hamiltonian operator. Ψ is the wave-function.

It states that for any trial wave function the energy calculated will always be equal to or greater than the energy of the true wave function. Improving the trial wave-function depends on finding parameter values that result in the lowest possible expectation value. For the Hartree-Fock method the atomic orbital coefficients (C) from equation 8 (previous page) are the parameters and from equations 8 and 9 (previous page) Φ_i is the trial wave-function with electronic energy (E_i) as the expectation value. Following along with Figure 20 (next page), first the algorithm starts with the basis set and input of the three-dimensional coordinates of the nuclei.[29] From this an initial guess wave function is made and an initial probability density is determined. This density matrix is then used to form a Fock matrix (and thus the secular determinant). Diagonalization of this Fock matrix then permits the construction of an updated density matrix. If the new density matrix is sufficiently similar in energy to the previous density matrix then then the SCF cycle is converged. If not then the new density matrix is used to construct and solve a new Hartree-Fock secular equation until the new density matrix is sufficiently similar to the previous density matrix used to form the Fock matrix, hence the name Self-Consistent Field. After SCF convergence, then the molecular geometry optimization occurs based off its location on the potential energy surface as described in Chapter 1 (pages 13-14), determining if it is either a transition state or energy minimum by analysis of the local surface. If the geometry does not correspond to either, then a new modified geometry is chosen to push it along the potential energy surface toward its optimization criteria. This new geometry then goes back into the SCF cycle.

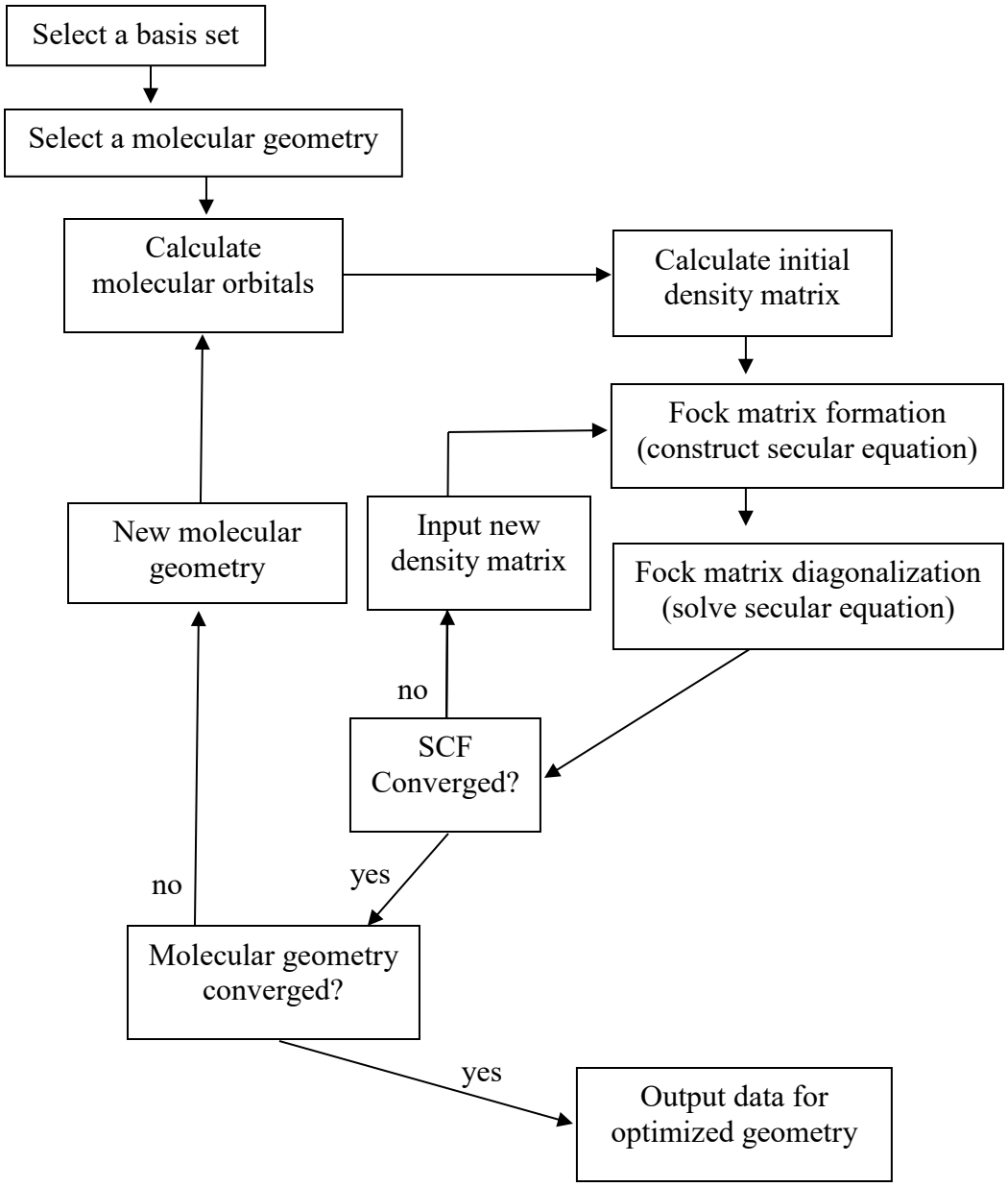

Figure 20. Flow chart illustrating the Hartree-Fock Self Consistent Field procedure.

Sometimes submitted jobs find themselves in a Sisyphean computational purgatory. In which case, if after a certain number of attempts a job fails to converge the calculation is deemed to have run out of steps and is terminated, in order preclude a job from running indefinitely. When the criteria for convergence is nearly met but falls

slightly short then a frequent source of computational purgatory is an algorithmic overcorrection in the next cycle, resulting in an oscillation around the convergence criteria but never landing on the target. This a frequent source of malaise and existential terror in a computational chemist's life when trying to find transition state structures.[54] Keywords can be added to the job's route section to modify the calculation and aid in dealing with these nightmarish scenarios, such as increasing the number of cycles to give the calculation more attempts to hone in on the convergence criteria.[55] Another option is to change the step size. This affects the extent of the algorithmic correction due to the magnitude in which orbital coefficients termed "Fock space" are modified. A final option that can be employed is loosening the convergence criteria itself and manually changing the output geometry to then resubmit a new job in hopes of reaching the promised land. Alternatively, sometimes a job meant to optimize a minimum structure will optimize to a transition state in which case tightening the convergence criteria will help ensure the appropriate convergence to the specified type of structure within the potential energy surface.

Complete Active Space Self-Consistent Field Theory

Complete Active Space Self-Consistent Field (CASSCF) theory is a post-Hartree-Fock method that builds upon the HF method by employing a linear combination of configuration state functions to approximate the electronic wave-function as seen in equation 11 (next page).[29] Each configuration state is represented by a determinant and its contribution to the total wave-function is weighted by coefficient *c*.

$$\Psi = c_0\Psi_{HF} + c_1\Psi_1 + c_2\Psi_2 + \cdots$$

Equation 11. Linear combination of configuration state functions. Ψ is the total electronic wave function. $\Psi_{HF,1,2,\ldots}$ are the individual configuration state functions (CSF). c is a coefficient that weights the contribution of each CSF.

Going back to Hartree-Fock theory, electrons are treated as moving independently through a static electric field created by all electrons and then optimizes the molecular orbitals in a "self-consistent fashion" by variational method. Furthermore, the Fock operator is not a single operator, but rather the set of all the interdependent one-electron operators employed in calculating the one-electron molecular orbitals used in constructing the HF wave-function as a single slater determinant. The point of the variational method is to produce the closest possible wave-function representing the system of study to that of the true wave-function by minimizing the electronic energy. Thus, a conceptually straightforward approach toward improving the wave-function is to construct it out of rather than a single determinant, to construct it as a linear combination of multiple determinants. With each determinant representing a configuration state, in which the coefficient *c* weights the contribution of each state in the expansion normalization is ensured. A full configuration interaction with an infinite basis set is an exact solution Schrödinger equation (non-relativistic, time-independent, Born-Oppenheimer).[29] As illustrated in Figure 21, this would completely account for the electron correlation that the Hartree-Fock method neglects. Unfortunately, for those constrained by the limits of reality, a full configuration interaction with an infinite basis set would also take an infinite amount of time to calculate and is thus infeasible.

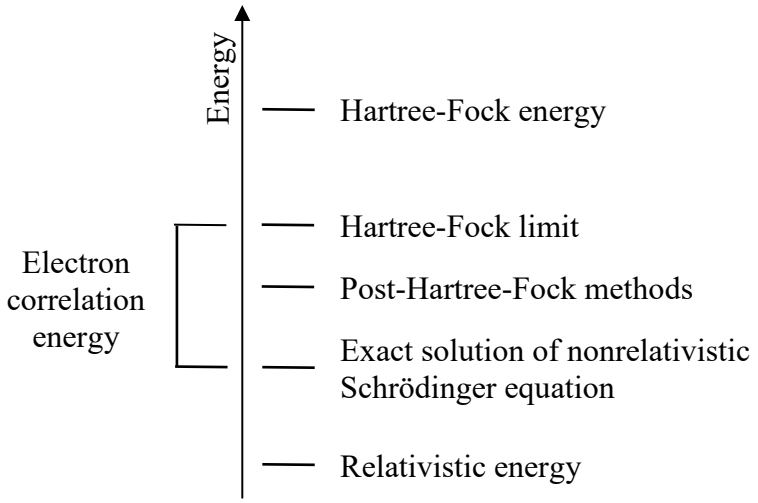

Figure 21. Diagram qualitatively illustrating the improvement by post-Hartree-Fock methods in calculating a systems energy.

The computational time of a CASSCF calculation will also greatly depend on the number of orbitals (*n*) and electrons (*m*) within the defined active space.[29] Equation 12 below shows the number (*N*) of individual singlet configuration state functions (CSF) derived from an active space comprised of *m* electrons and *n* orbitals.

$$N = \frac{n!\,(n+1)!}{\left(\frac{m}{2}\right)!\left(\frac{m}{2}+1\right)!\left(n-\frac{m}{2}\right)!\left(n-\frac{m}{2}+1\right)!}$$

Equation 12. *N* is the number of singlet state CSFs. *n* is the number of orbitals. *m* is the number of electrons.

For example, to do a full configuration interaction for every single electron in formaldehyde would result in 3.48×10^7 CSFs. Based off the time it takes Grizzly to perform one HF/6-31G(d) single-point energy calculation for formaldehyde it is estimated that the full configuration interaction calculation would take a little over eleven years. 1,3-dioxetane would result in 4.13×10^{16} CSFs and is estimated to take over 13

million millennia to complete. To keep the computational time reasonable, the active space is restricted. This type of calculation is termed a multi-configuration self-consistent field calculation (MCSCF). Inside the restricted active space a Slater determinant is generated for every possible occupation scheme by a specified number of orbitals and electrons (*n*,*m*). By default, the specified orbitals and electrons are split evenly across the HOMO/LUMO called the "frontier". In the rest of the restricted active space above and below the HOMO/LUMO orbitals no more than *n* excitations above the complete active space are permitted. Below and above the restricted active space electrons are respectively enforced to be doubly occupied and unoccupied, respectively. Above and below those are then frozen HF orbitals. Figure 23 (next page) illustrates this for a (4,4)-MCSCF calculation of formaldehyde.

Considering the example of formaldehyde dimerizing to form either 1,2- or 1,3-dioxetane via [2+2] cycloaddition. The π-bonds break to form the two new σ-bonds as seen in figure 22 below.

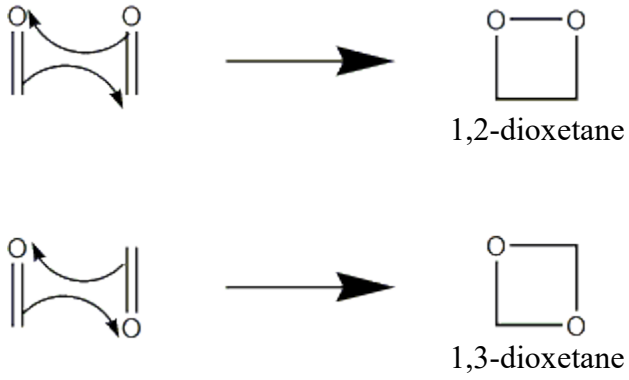

Figure 22. [2+2] cycloaddition of formaldehyde to 1,2- and 1,3-dioxetane.

To model this reaction the active space is defined by 4 electrons in 4 orbitals: a (4,4) MC-SCF calculation. Ideally, this includes the 4 electrons occupying the carbon-oxygen π –bond and σ –bond as well as the π* and σ* orbitals.

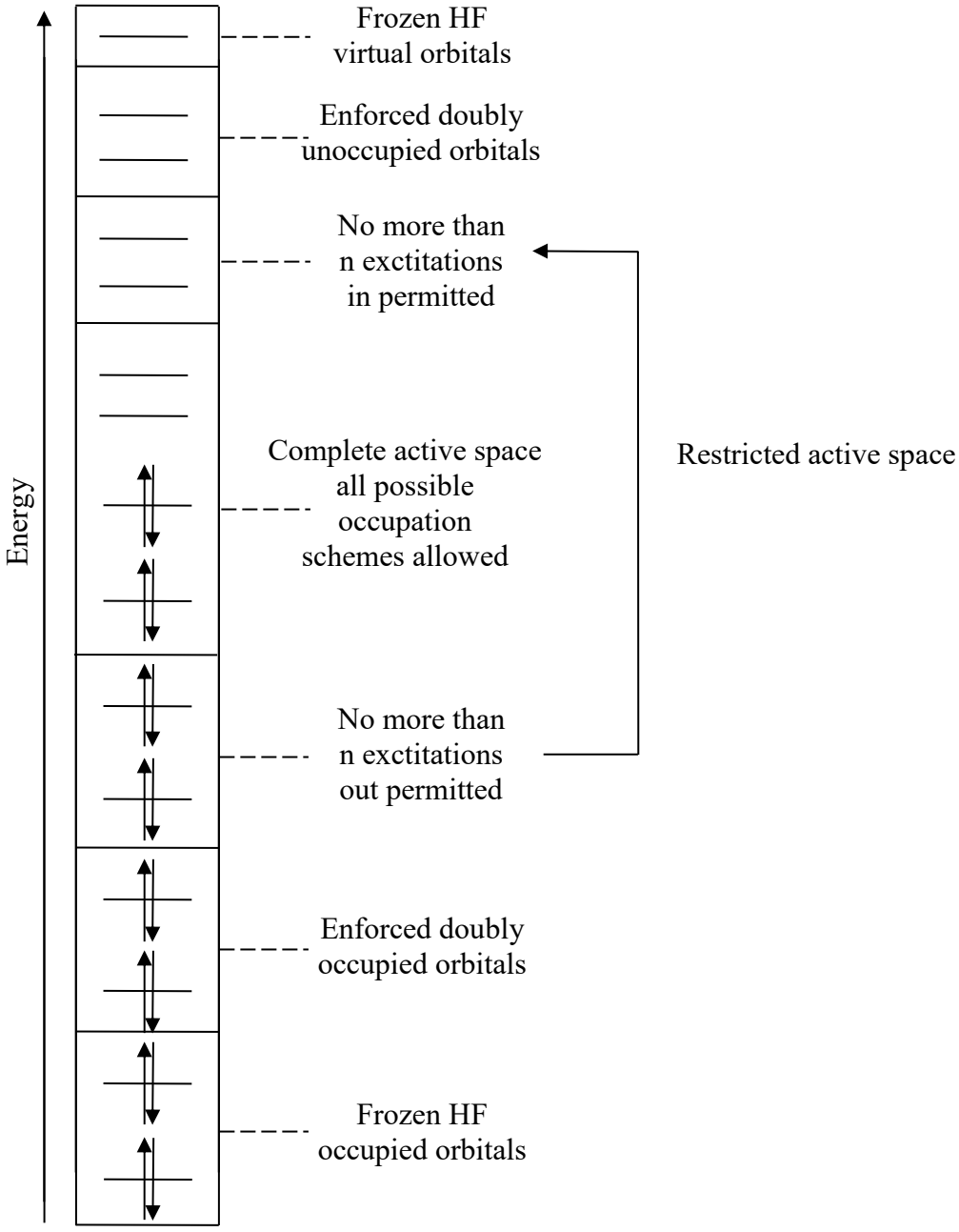

Figure 23. Visual depiction of the ground state configuration of a (4,4)-MCSCF calculation for formaldehyde.

As previously mentioned the active space by default is divided evenly across the HOMO/LUMO "frontier". As seen in Figure 24 and 25, respectively (on pages 39 and 40) that the π and π* orbitals are in the HOMO/LUMO whereas the σ and σ* orbitals are not.

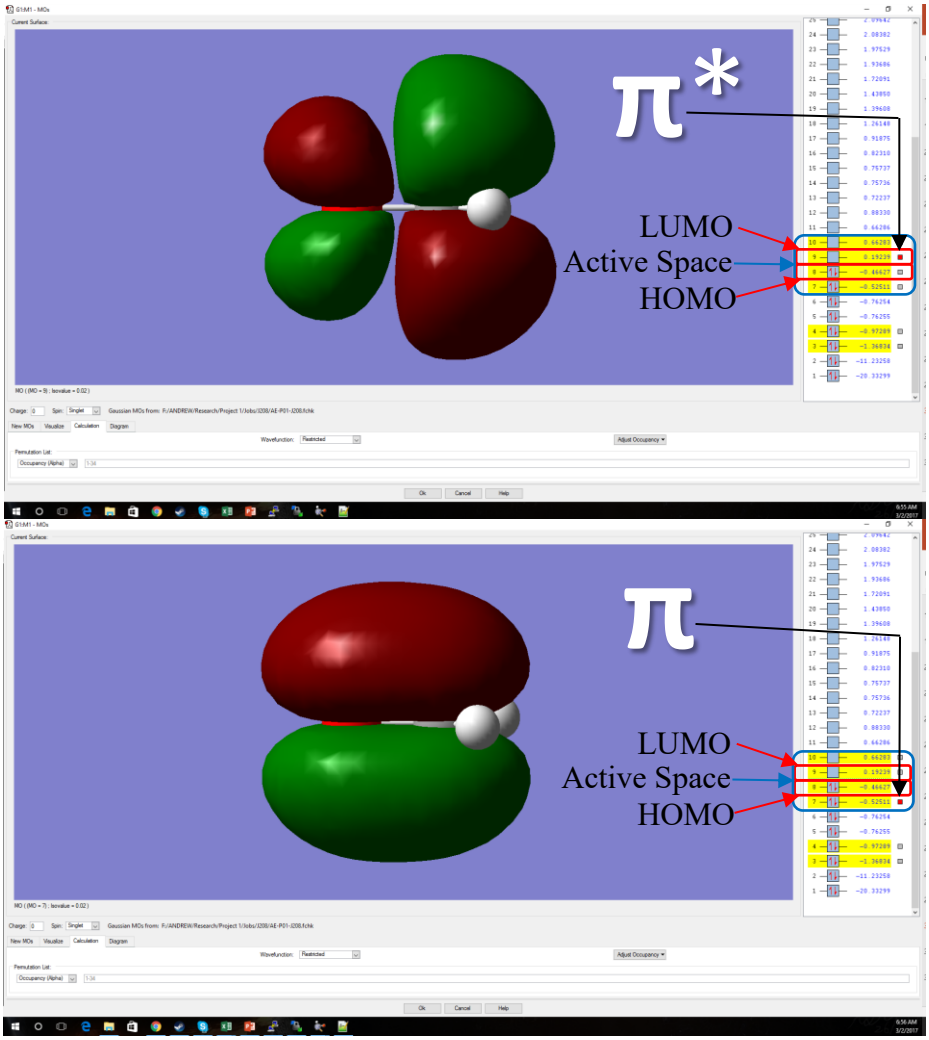

Figure 24. (4,4)-MCSCF molecular orbital specification π and π*. The π and π* orbitals of formaldehyde are found within the active space and do not need to be specified.

When creating the calculation, one can further specify the active space by swapping out the two unwanted orbitals. Performing any MCSCF calculation requires extensive orbital analysis, typically a combination of natural bond order analysis and visual orbital inspection.

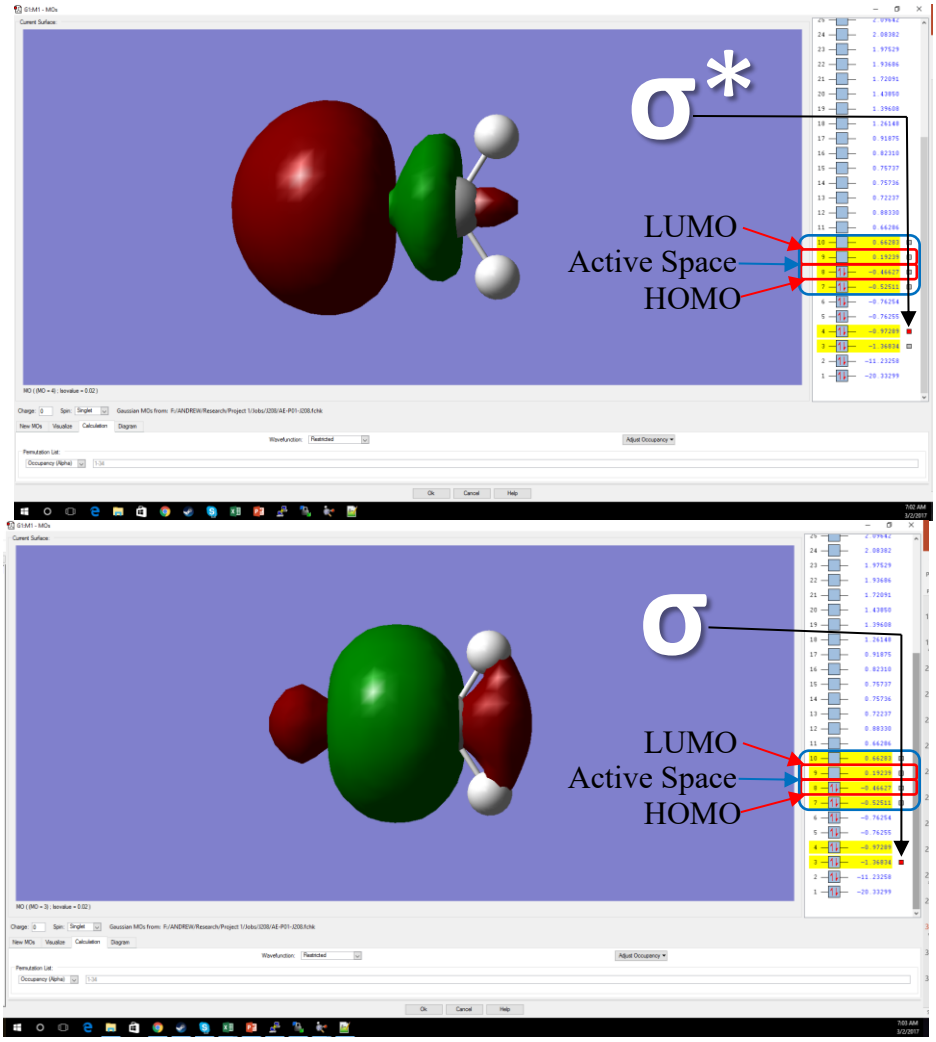

Figure 25. (4,4)-MCSCF molecular orbital specification σ and σ*. The σ and σ* orbitals of formaldehyde are found outside the active space and need to be specified.

Density Functional Theory

The roots of density functional theory (DFT) stretch back to 1927, the same year that Douglas Hartree proposed his iterative method for solution of the Schrödinger equation.[29] However, it was not until much later that DFT would see much use outside of solid state physics research.[56] The Thomas-Fermi DFT model proposed that instead of using a wave function to describe a quantum mechanical system, which requires (for an N electron problem) $3N$ spatial coordinates and N spin variables, to instead just use the electron density of the system (ρ). This progenitor to modern DFT is of historical importance. However, it's accuracy in describing chemical systems was severely limited as it only approximated kinetic energy. Furthermore, it wasn't for another year until 1928 that Paul Dirac modified the Thomas-Fermi model to include a term for electron exchange. Even still the model completely neglected to account for electron correlation.

The rigorous conceptual basis for modern DFT came in 1965 with the publication of the Hohenberg-Kohn existence theorem and variational theorem.[57] The existence theorem states that the external potential is a unique functional of the electron density. This in turn results in a Hamiltonian and wave function that yields a unique energy in accord with that specific density. Additionally, the variational theorem states that an electron density can also be subject to the variational principle, and by which refine a trial density to minimize the energy of a described system, as any trial density will always be higher than or equal to the energy of that for the true density. In the following year, Walter Kohn and Lu Jeu Sham published a method for DFT similar to that of the Hartree-Fock method. This new method hinged around non-interacting orbitals (termed Kohn-Sham orbitals) in which each electron experiences an averaged external potential.

Effectively this substitutes a full interacting system with real potential for a fictitious non-interacting system allowing electrons to move with an effective single particle potential. A breakdown of the total energy of the Kohn-Sham noninteracting orbital system is given in equation 13 below.[56]

$$E[\rho] = T_s[\rho] + \int [V_{ext}(r) + J(r)]\rho(r)dr + E_{xc}[\rho]$$

Equation 13. Breakdown of Kohn-Sham total energy. $T_s[\rho]$ is kinetic energy. V_{ext} is the external potential. *J(r)* is the coulomb interaction. E_{xc} is the exchange correlation.

The ground state density of the real system matches exactly the density yielded by the Kohn-Sham method.[56] However, the ability to determine an exact solution is limited by the difficulty in expressing the exchange-correlation energy (E_{xc}). A biblical analogy to Jacob's ladder has been drawn in representing a series of approximations attempting to solve the issue of representing E_{xc}.[58] In Genesis 28:10-19 Jacob's ladder represents a path from earth to heaven, on the following page Figure 26 illustrates this analogy in which the lowest rung represents the least accurate DFT method of representing E_{xc} and the highest rung the most accurate.[59,60] The first attempt at better modeling E_{xc} came from employing a uniform gas as the electron density termed the local density approximation (LDA). The next rung up employs dependence on the gradient of the density termed the generalized gradient approximation (GGA). The following rung up were originally DFT functionals that included the second derivative of the electron density (the Laplacian).[61] Today they are characterized by including a dependence on the kinetic energy density. The last two rungs are hybrid and double hybrid DFT functionals.[60] Both include a hybrid

description of exchange using HF exchange in addition to DFT exchange. The primary difference between hybrid and double hybrid is that hybrid functionals are dependent on occupied orbitals while double hybrid functionals are dependent on occupied and virtual orbitals. Additionally, double hybrid functionals include correlation from wave-function theory. As one goes up Jacob's ladder of DFT the chemical accuracy increases but so, too, does the computational cost.

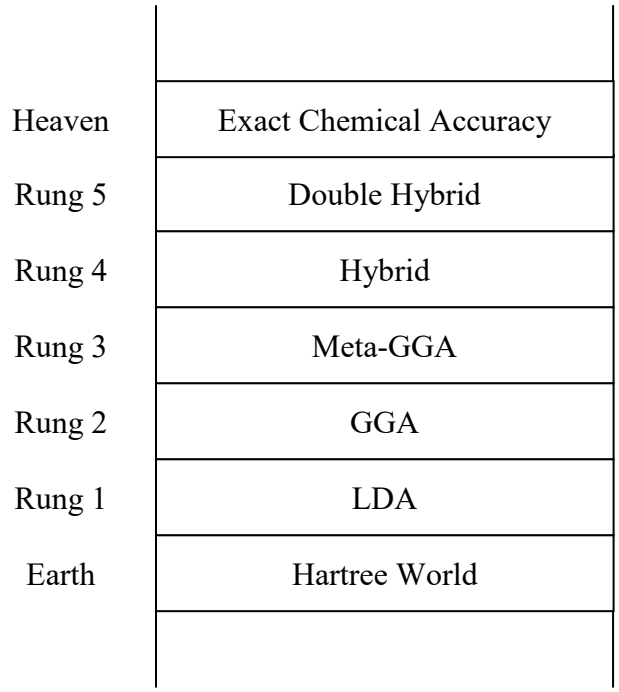

Figure 26. Perdew's DFT Jacob's Ladder.[58] Ascending the rungs of Jacobs ladder increases chemical accuracy at the price of also increasing computational cost.

The DFT functional used in this study is B3LYP, a hybrid functional. B3LYP stands for Becke's three-parameter exchange Lee, Yang and Parr's correlational functional. A hybrid functional is constructed as a linear combination of correlation and exchange density functionals along with the Hartree-Fock exact exchange functional.[56]

The parameters defining the weight of each individual functional are set by tuning the functionals predictions to fit with prior empirical data.[62] Examples of which include empirical data regarding atomization energies, ionizations potentials, proton affinities and atomic energies.[56] Equation 11 below shows the breakdown of the B3LYP exchange-correlation into its Hartree-Fock exact exchange, density correlational and density exchange functionals.[63]

$$E_{xc}^{B3LYP} = E_x^{LDA} + a_0(E_x^{HF} - E_x^{LDA}) + a_x(E_x^{GGA} - E_x^{LDA}) + E_c^{LDA} + a_c(E_c^{GGA} - E_c^{LDA})$$

Equation 11. Breakdown of the B3LYP exchange-correlation. Functionals are weighted a_0=0.20, a_x=0.72 and a_c=0.81. *x* represents exchange energy. *c* represents correlation energy.

Unrestricted Calculations

By default, all calculations are restricted if not specified otherwise.[29] Restricted calculations enforce double occupation of α and β spin electrons to the same orbital. Restricted calculations are implemented by utilizing one molecular orbital twice multiplying one by the α spin function and the other identical orbital multiplied by the β spin function in the Slater determinant. Whereas in an unrestricted calculation α and β spin electrons are calculated with different orbitals. This results in an unrestricted calculation having separate operators in the SCF cycle, one for the α electrons and one for the β electrons. Because of this unrestricted calculations had originally been called DODS calculations (different orbitals for different spins).[64] Today the nomenclature in use is unrestricted versus restricted and is represented by a "*u*" in front of the functional (e.g. uMP2 or uB3LYP).

Spin, being a molecular property, can be calculated from the wave function describing a given system as seen below in Equation 12 where $\hat{S}^2$ is the total spin operator.[29]

$$\langle \Psi | \hat{S}^2 | \Psi \rangle = \langle S^2 \rangle$$

Equation 12. $\hat{S}^2$ is the total spin operator. Ψ is the wave function. S^2 is the spin eigenvalue.

When performing an unrestricted calculation it is important to consider the possibility of spin contamination. That is the introduction of higher order spin states. Equation 13 below calculates the exact eigenvalues for equation 12.

$$S(S+1) = S^2$$

$$0(0+1) = 0$$

$$0.5(0.5+1) = 0.75$$

$$1(1+1) = 2$$

Equation 13. Correct spin eigenfunction values for singlet (S^2=0), doublet (S^2=0.75) and triplet (S^2=2) states where S is the cumulative spin of +1/2 or -1/2 for α and β spin electrons.

Deviation from those values listed above for the respective spin states is indictitive of spin contamination. An unrestricted calculation will always yield an S^2 value equal to or greater than the exact eigenvalue for that spin state depending on the extent to the spin contamination. This is considered problematic as it does not represent a real empirical analog and is chemically inaccurate. A commonly cited rule of thumb for working with organic molecules, is that if the spin contamination is 10% or less from the expected S^2 value then it is negligible.[64] Despite the issues of spin contamination unrestricted

calculations are valuable in that they are necessary for modeling unpaired electrons and incorporating spin polarization. Unrestricted calculations sometime yield lower energies due to having greater variational freedom. However more often than not they result in higher energy calculations due the inclusion of higher order spin states.[64]

CHAPTER 5: RESULTS

Experimental scheme

The following experimental results are laid out into two sections following the path of the modeled reaction; intermediate formation and sulfur extrusion. To moderate computational cost the cycloaddition will be studied with the homodimerization of ethylene, formaldehyde and thioformaldehyde to form cyclobutane and 1,2-/1,3-dioxetane and -dithietane as intermediate analogs. 1,2-/1,3- dioxetane and -dithietane structures are then taken through sulfur extrusion. Figure 27 below illustrates this experimental scheme.

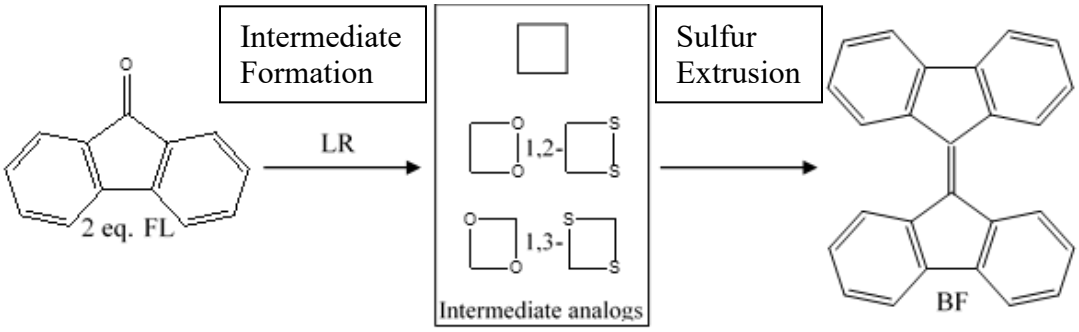

Figure 27. Schematic of computational analysis for the dimerization of fluorenone to 9,9'bifluorenylidene using an analog system. Fluorenone is substituted with ethylene, formaldehyde and thioformaldehyde to form the intermediates cyclobutane, 1,2-/1,3-dioxetane and dithietane. Formation of intermediates is followed by subsequent extrusion pathways for the 1,2-dioxetane and –dithietane structures.

Though it is possible to envision other mechanisms that could lead to the proposed 1,2- and 1,3- intermediates, this study instead chooses to opt for Occam's razor and examine stepwise and concerted pathways to (2+2) cycloadducts. Figures for the first section examining 1,2-/1,3- intermediate formation are organized by the transition state structures (TSS), starting with supra-supra (SS), followed by supra-antara (SA) and

ending with an examination of stepwise mechanisms. The second section looks at two different pathways by which sulfur extrusion may occur yielding diatomic sulfur and ethylene. The first pathway is a simple stepwise ionic bond cleavage of the first and second carbon sulfur bonds. The second pathway starts with a concerted rearrangement of the 1,2-dithietane to a thiirane structure in which the other sulfur is bonded to the heterocyclic sulfur hanging off the three membered ring followed by a concerted extrusion of diatomic sulfur. Calculations were performed using the restricted and unrestricted DFT functional B3LYP as well as (4,4) & (8,8)-CASSCF. All calculations used the basis set 6-31G(d). All stationary point energies are reported in kcal/mol with zero-point energy correction added relative to the energy of the corresponding reactants. All transition states have been connected to their corresponding energy minima in either the forward or reverse direction by IRC and optimized to final geometry.

Intermediate Formation

Figures 28-30 depict a supra-supra [2+2] cycloaddition of formaldehyde forming 1,2-dioxetane and 1,3-dioxetane intermediate analogs using a restricted density functional theory model chemistry of B3LYP/6-31G(d). Figure 29 and 30 correspondingly depict the transition state structures forming 1,2-dioxetane and 1,3-dioxetane. The 1,2-dioxetane TSS has a larger energetic barrier as both electron rich oxygens approach each other resulting in electrostatic repulsion. Whereas the 1,3-dioxetane TSS has a lower energetic barrier owing to the electrostatically favorable interaction of electron rich oxygen atoms with electron poor carbon atoms.

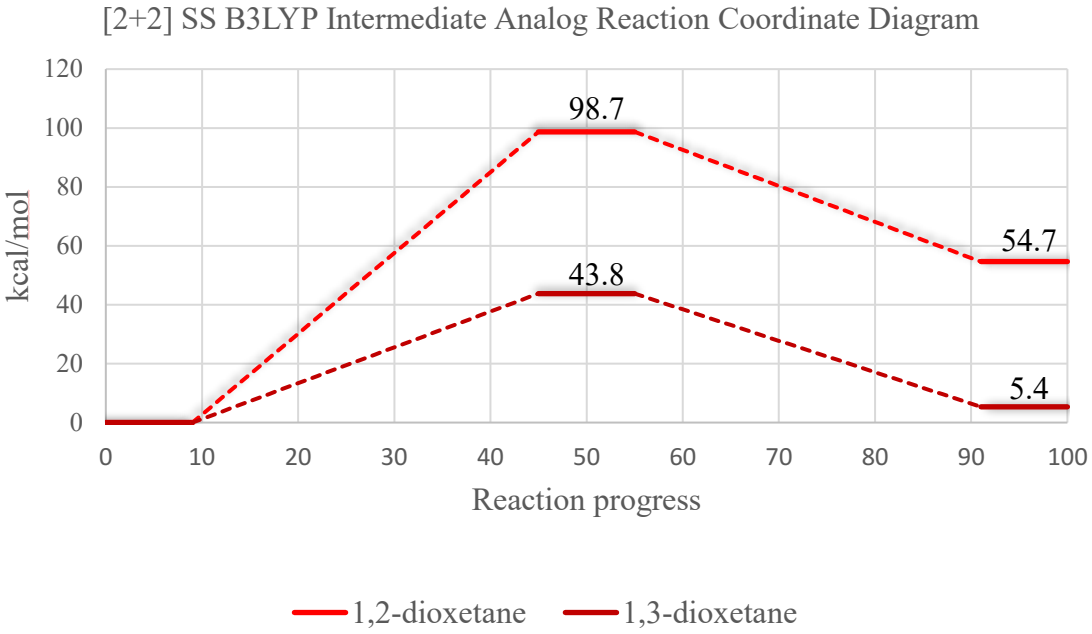

Figure 28. Reaction coordinate diagram of a supra-supra [2+2] cycloaddition of formaldehyde forming 1,2-dioxetane and 1,3-dioxetane intermediate analogs.

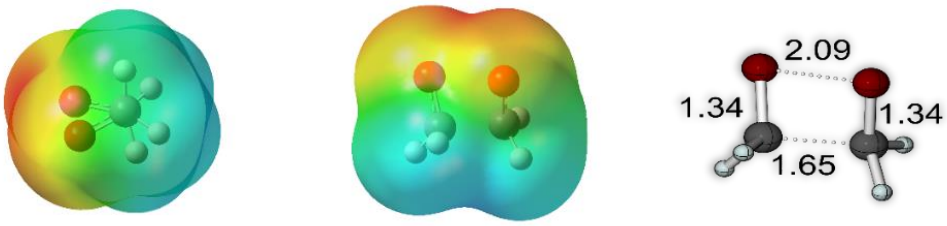

Figure 29. 1,2-dioxetane [2+2] SS B3LYP/6-31G(d) TSS. Electrostatic potential map and stationary point geometry. Isovalue -4.00e-2 to 4.00e-2. Distances in angstroms.

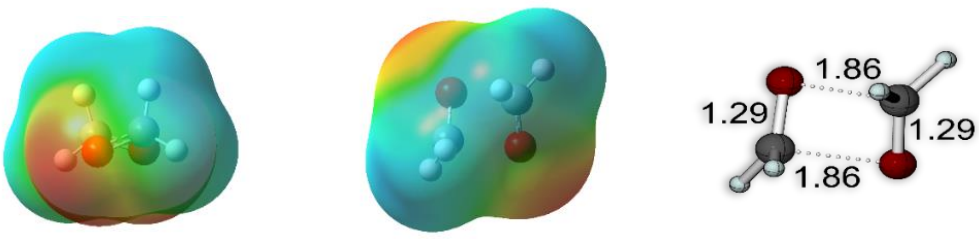

Figure 30. 1,3-dioxetane [2+2] SS B3LYP/6-31G(d) TSS. Electrostatic potential map and stationary point geometry. Isovalue -4.00e-2 to 4.00e-2. Distances in angstroms.

Figures 31-32 depict a supra-supra [2+2] cycloaddition of formaldehyde forming the 1,3-dioxetane intermediate using the wave-function based method CASSCF with a

6-31G(d) basis set. Figure 30 shows the transition state structure, which has a very similar structure to that seen in prior in Figure 30 however the electrostatic potential map shows a greater separation of charge, which may be responsible for the significantly higher energetic barrier. The calculation used a (4,4) active space for formaldehyde (x2) and an (8,8) active space for the transition state structure as well as 1,3-dioxetane following the π and σ bonds involved as detailed in the methods section.

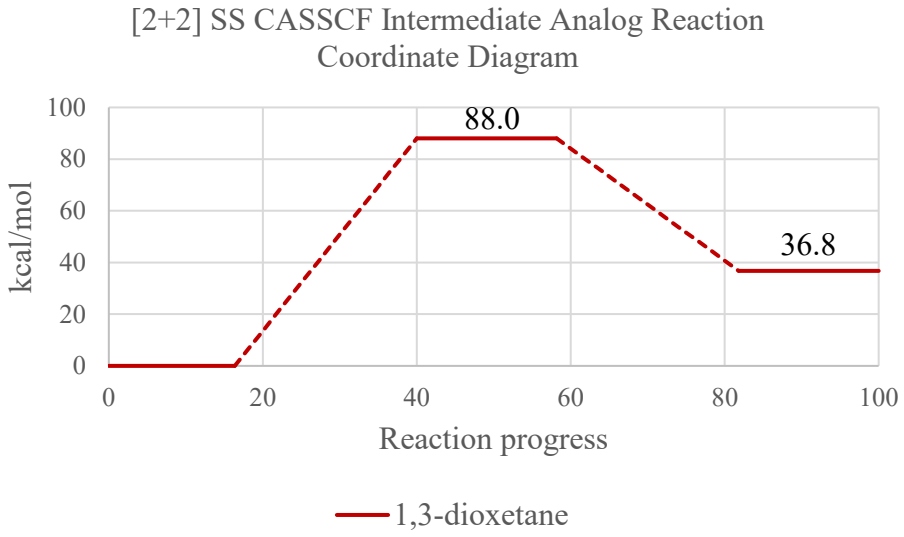

Figure 31. Reaction coordinate diagram of a supra-supra [2+2] cycloaddition of formaldehyde forming the 1,3-dioxetane intermediate analog. Calculation used a (4,4) active space for formaldehyde (x2) and an (8,8) active space for the transition state structure and 1,3-dioxetane.

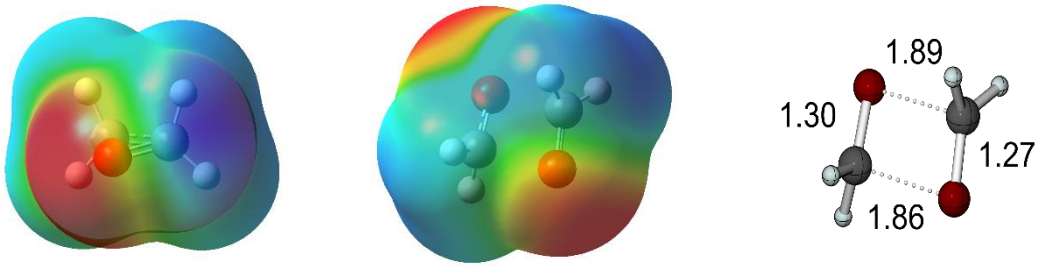

Figure 32. 1,2-dioxetane [2+2] SS CASSCF/6-31G(d) TSS. Electrostatic potential map and stationary point geometry. Distances in angstroms.

Figures 33-36 depict a supra-supra [2+2] cycloaddition of formaldehyde forming 1,2-dioxetane and 1,3-dioxetane intermediate analogs and a supra-supra [2+2] cycloaddition of thioformaldehyde forming 1,2-dithietane using an unrestricted density functional theory model chemistry of uB3LYP/6-31G(d). The 1,3-dioxetane TSS has an S^2 value of exactly 0 making it identical to the prior restricted B3LYP 1,3-dioxetane TSS from Figure 26 and 28. Whereas the 1,2-dioxetane and 1,2-dithietane TSS show significant spin contamination with total spin values of S^2=1.005537 and S^2=0.98202 indicating a higher order spin state corresponding to a similar nuclear geometry contaminating the unrestricted calculation.

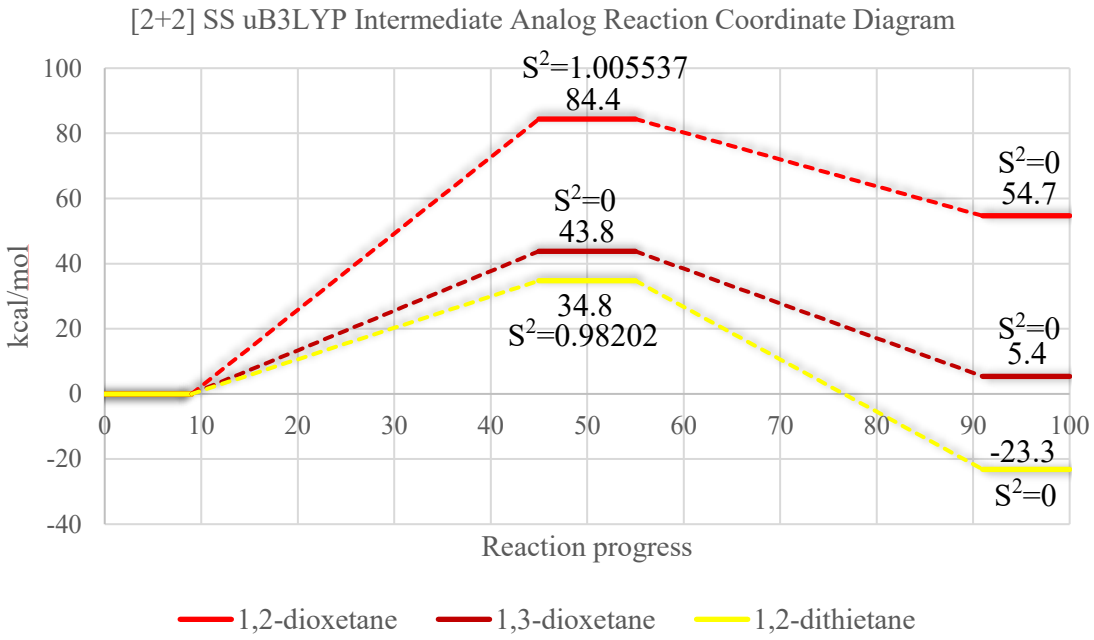

Figure 33. Reaction coordinate diagram of a supra-supra [2+2] cycloaddition of formaldehyde forming 1,2-dioxetane and 1,3-dioxetane intermediate analogs as well as thioformaldehyde forming a 1,2-dithietane intermediate analog.

Figures 34-35 support a rationalization in energy difference by 1,3-dioxetanes head to tail approach as seen previously compared to 1,2-dioxetane. However, 1,2-

dithietane has a more diffuse distribution of electron density resulting in a lower energetic reaction barrier than either 1,2-dioxetane or 1,3-dioxetane.

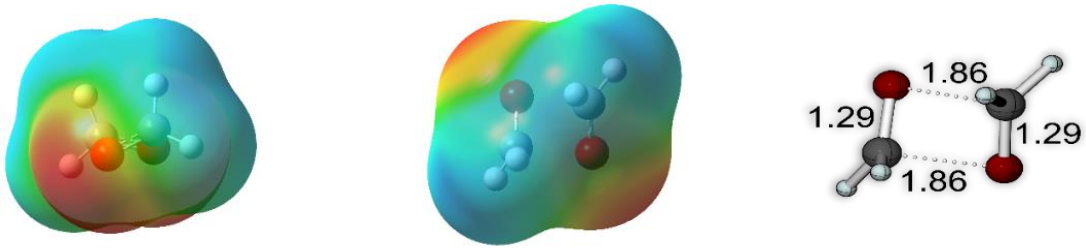

Figure 34 . 1,2-dioxetane SS TSS uB3LYP/6-31G(d). Electrostatic potential map and stationary point geometry. Isovalue -4.00e-2 to 4.00e-2. Distances in angstroms.

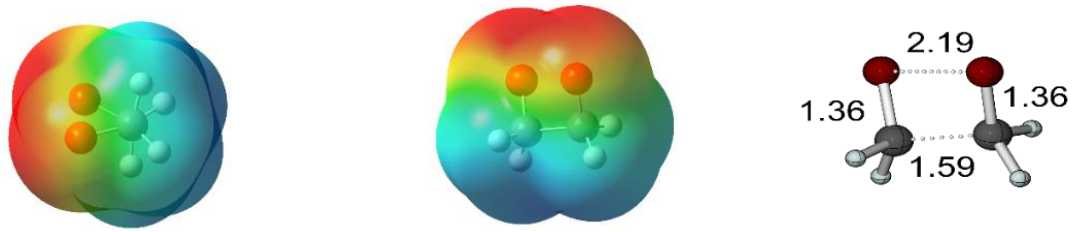

Figure 35. 1,2-dioxetane SS TSS uB3LYP/6-31G(d). Electrostatic potential map and stationary point geometry. Isovalue -4.00e-2 to 4.00e-2. Distances in angstroms.

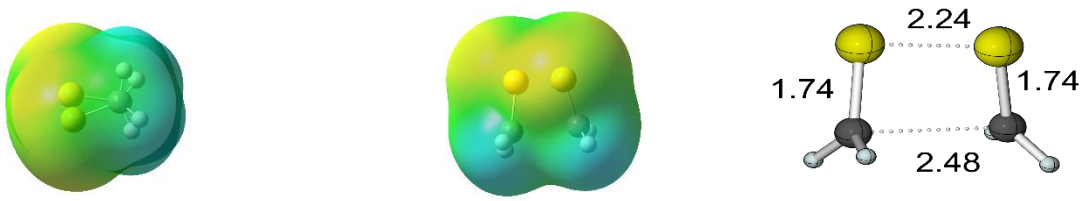

Figure 36. 1,2-dithieetane SS TSS uB3LYP/6-31G(d). Electrostatic potential map and stationary point geometry. Isovalue -4.00e-2 to 4.00e-2. Distances in angstroms.

Figures 37-41 depict a supra-antara [2+2] concerted asynchronous cycloaddition forming intermediate analogs cyclobutane, 1,3-dioxetane and 1,2-dithietane. Formation of cyclobutane and the higher energy 1,3-dithietane TSS were located using a restricted density functional theory model chemistry of B3LYP/6-31G(d). Whereas formation of 1,3-dioxetane and the lower energy 1,3-dithietane TSS were located using an unrestricted density functional theory model chemistry of uB3LYP/6-31G(d). The 1,3-dioxetane TSS

has an S^2 value of exactly 0 meaning that is exactly a closed shell singlet with no contamination. The unrestricted 1,2-dithietane TSS has significant spin contamination from a higher order spin state. All of the transition states are concerted asynchronous, presumably with the first σ-bond formed by initial constructive overlap between *p*-orbitals then having the other pair of orbitals interacting deconstructively requiring one of them to rotate to form the second σ-bond. This supra-antara [2+2] cycloaddition proceeds in a concerted but asynchronous manner with formation of the first σ-bond proceeding slightly before and during formation of the second σ-bond.

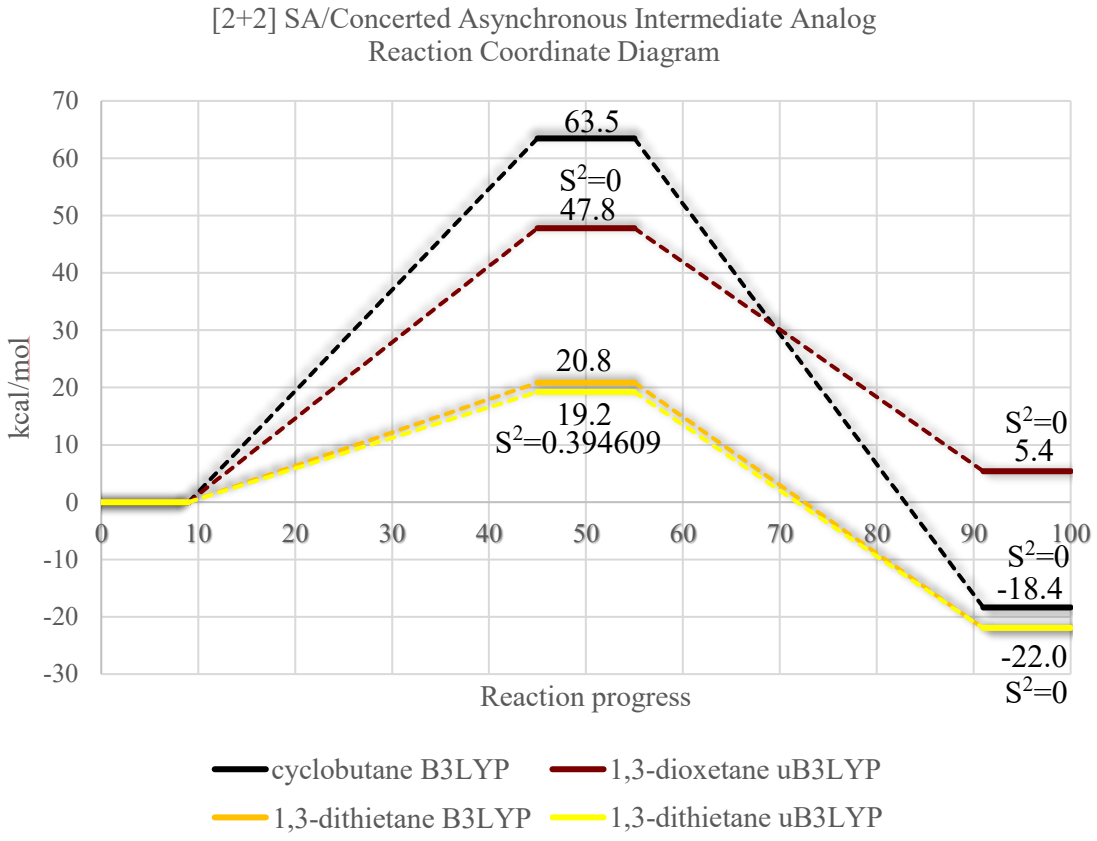

Figure 37. Reaction coordinate diagram of a supra-antara [2+2] cycloaddition of ethylene to cyclobutane, formaldehyde forming a 1,3-dioxetane intermediate analog as well as thioformaldehyde forming 1,2-dithietane intermediate analogs.

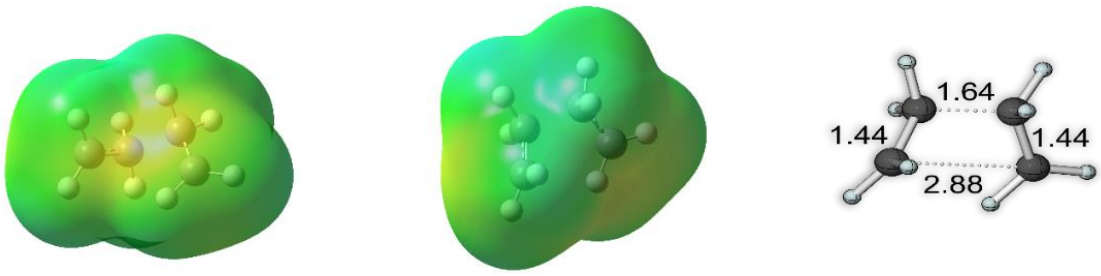

Figure 38 . 1,2-dioxetane SA TSS B3LYP/6-31G(d). Electrostatic potential map and stationary point geometry. Isovalue -4.00e-2 to 4.00e-2. Distances in angstroms.

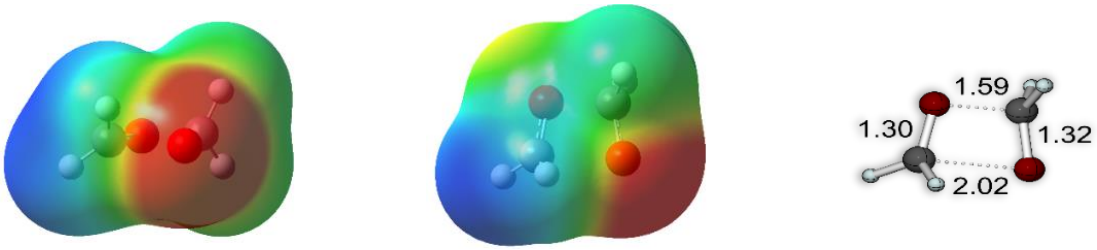

Figure 39. 1,2-dioxetane SA TSS uB3LYP/6-31G(d). Electrostatic potential map and stationary point geometry. Isovalue -4.00e-2 to 4.00e-2. Distances in angstroms.

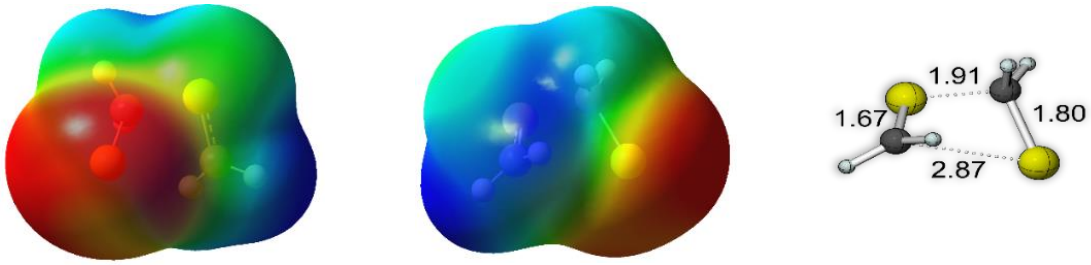

Figure 40. 1,2-dioxetane SA TSS B3LYP/6-31G(d). Electrostatic potential map and stationary point geometry. Isovalue -4.00e-2 to 4.00e-2. Distances in angstroms.

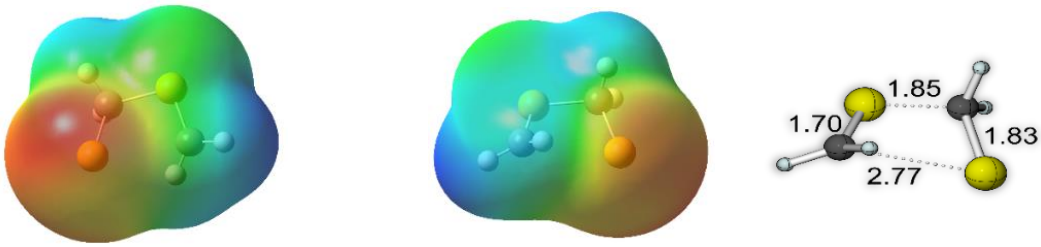

Figure 41. 1,2-dioxetane SA TSS uB3LYP/6-31G(d). Electrostatic potential map and stationary point geometry. Isovalue -4.00e-2 to 4.00e-2. Distances in angstroms.

Figures 42-50 depict a complete stepwise formation of intermediate analogs cyclobutane and 1,3-dithietane and the first transition state structures in a two-step stepwise formation of 1,2-dioxetane and 1,2-dithietane calculated using an unrestricted density functional theory model chemistry of uB3LYP/6-31G(d). Figure 40 also includes all of the intermediate analogs in comparison of energetic stability calculated in a singlet state with an S^2 of exactly zero.

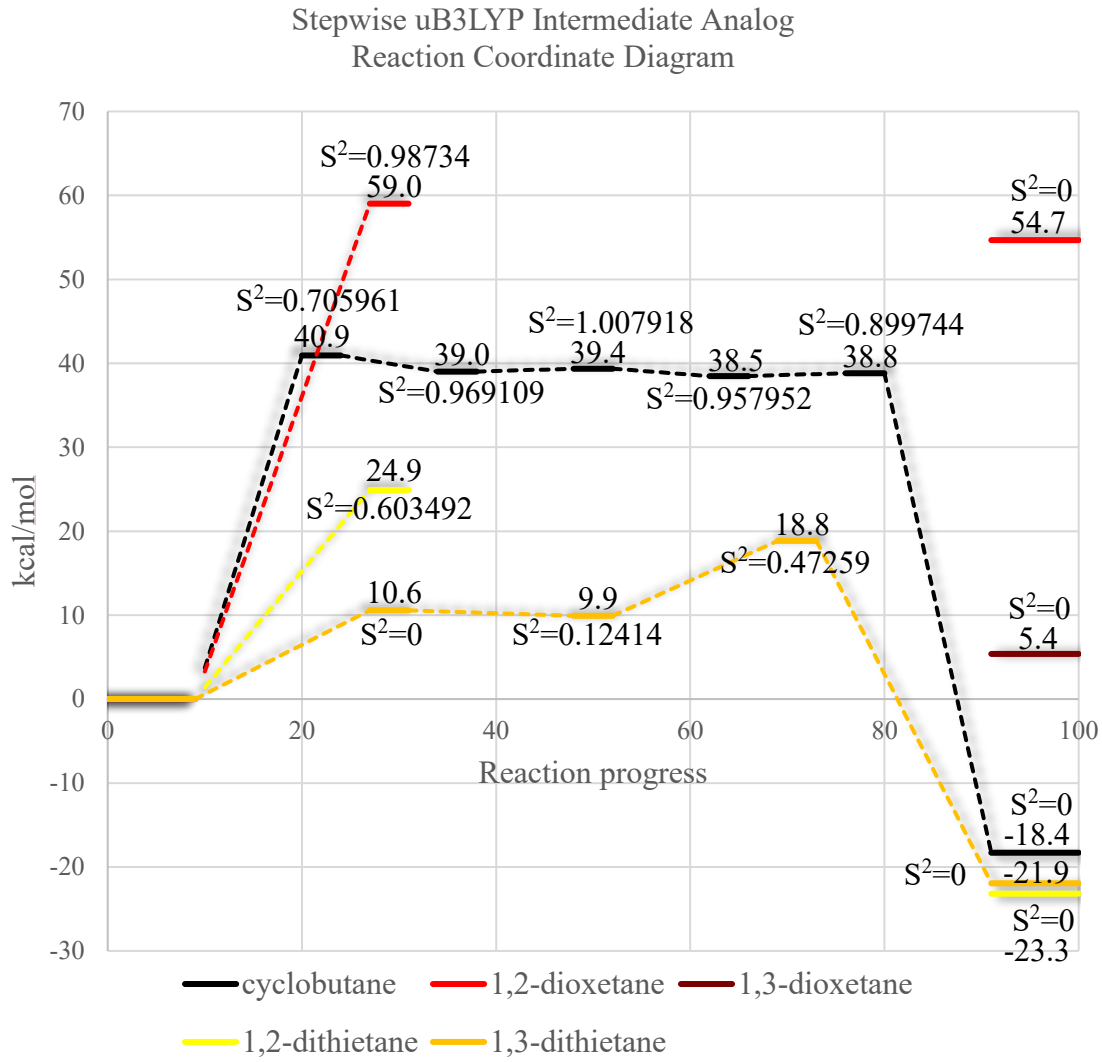

Figure 42. Reaction coordinate diagram of a full stepwise formation of cyclobutane and 1,3-dithietane intermediate analogs as well the first transition state in a two-step stepwise formation of 1,2-dioxetane and 1,2-dithietane intermediate analogs. On the right is a comparison of the energies of all five intermediate analog minima.

Stepwise formation of cyclobutane proceeds through three TSS. The first and last TSS correspond to formation of the first and second σ-bond. The second TSS corresponds to a rotation of both terminal carbons aligning the orbitals for constructive overlap. All TSSs and minima in this mechanism have significant spin contamination from higher order spin states.

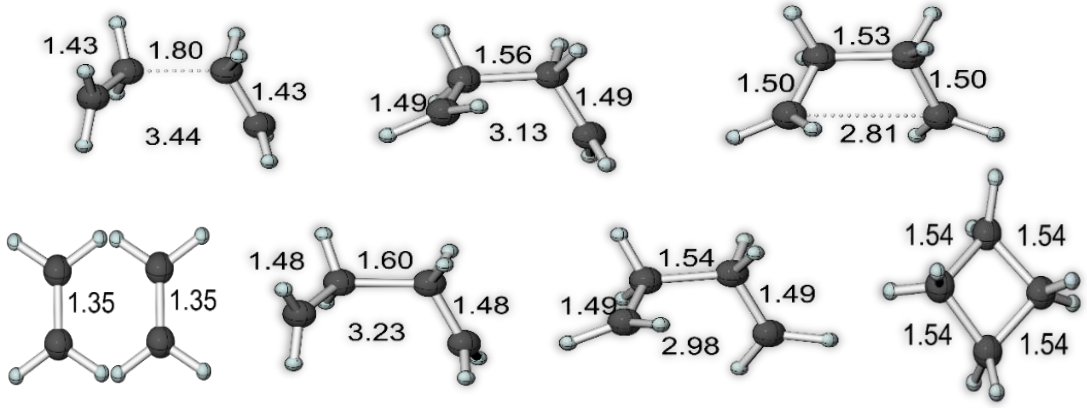

Figure 43. Ethene to cyclobutane formation uB3LYP/6-31G(d) stationary point geometries. Top row are transition states. Bottom row are minima. Distances in angstroms.

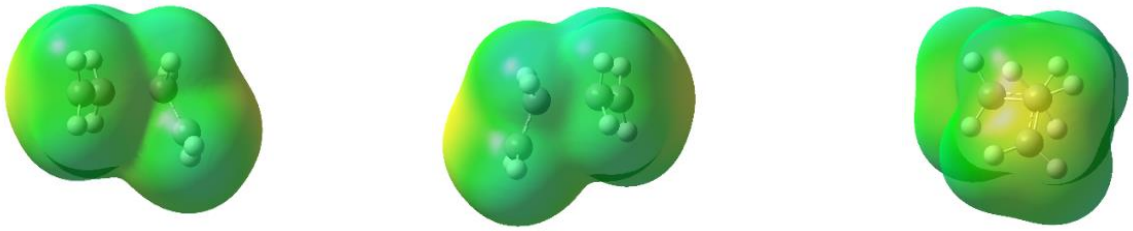

Figure 44. Cyclobutane TSS1 uB3LYP/6-31G(d). Electrostatic potential map. Isovalue -4.00e-2 to 4.00e-2.

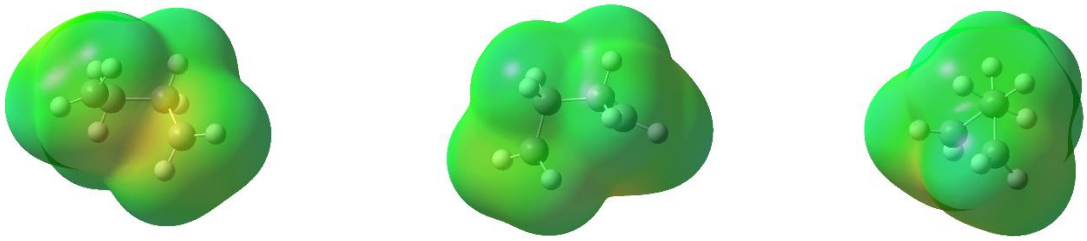

Figure 45. Cyclobutane TSS3 uB3LYP/6-31G(d). Electrostatic potential map. Isovalue -4.00e-2 to 4.00e-2.

Stepwise formation of 1,3-dithietane proceeds through two TSSs. The first TSS, a nucleophilic attack by the sulfur of one equivalent of thioformaldehyde on the electrophilic carbon of the other thioformaldehyde. The S^2 of the TSS is exactly zero indicating that the first step is ionic.

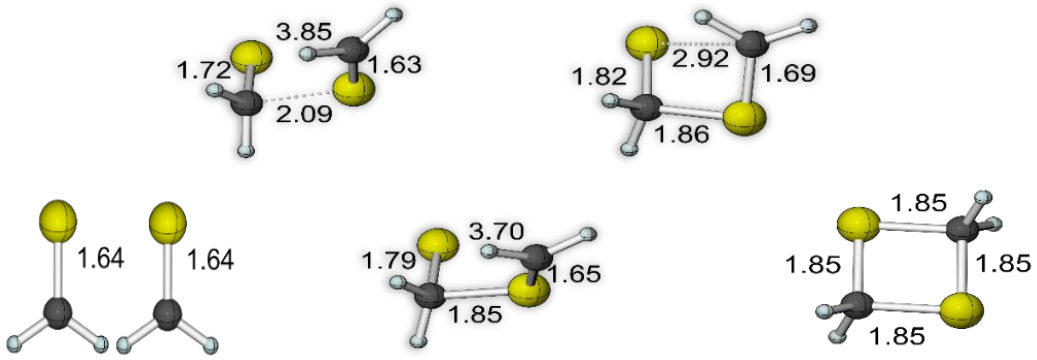

Figure 46. Thioformaldehyde to 1,3-dithietane formation uB3LYP/6-31G(d) stationary point geometries. Top row are transition states. Bottom row are minima. Distances in angstroms.

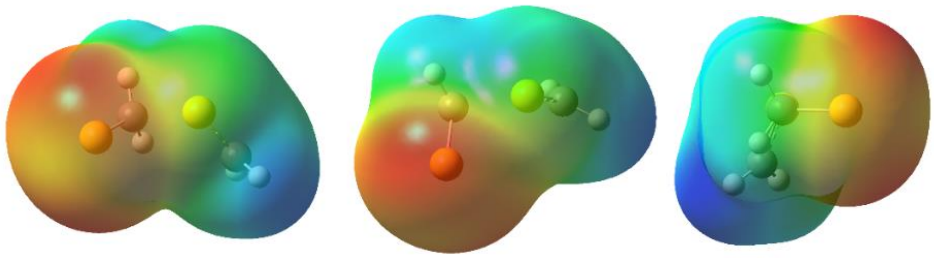

Figure 47. 1,3-Dithietane TSS1 uB3LYP/6-31G(d). Electrostatic potential map. Isovalue -4.00e-2 to 4.00e-2.

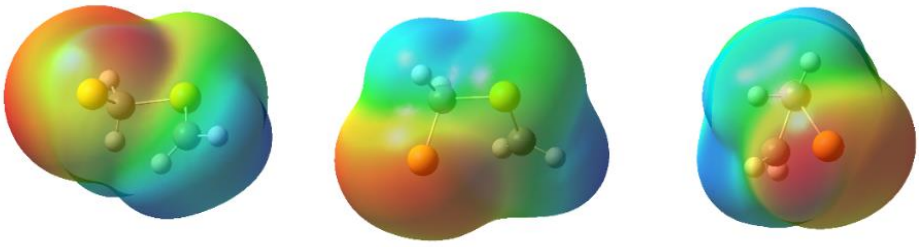

Figure 48. 1,3-Dithietane TSS2 uB3LYP/6-31G(d). Electrostatic potential map. Isovalue -4.00e-2 to 4.00e-2.

The second TSS in which the other two sulfur and carbon atoms form the second σ-sigma bond shows significant spin contamination from higher order spin states with a calculated total spin of 0.47259.

In examining a stepwise formation of 1,2-dioxetane and 1,2-dithietane, a first TSS was located for both in which the carbon atoms first form a bond. However, attempts to find the following TSS, in which either oxygen or sulfur atoms form the second and final bond, or a corresponding energy minimum connecting the first and second TSSs remain in a Sisyphean SCF cycle purgatory. It is important to note that both first transition states contain significant spin contamination from higher order spin states at S^2=0.9873 and S^2=0.603492.

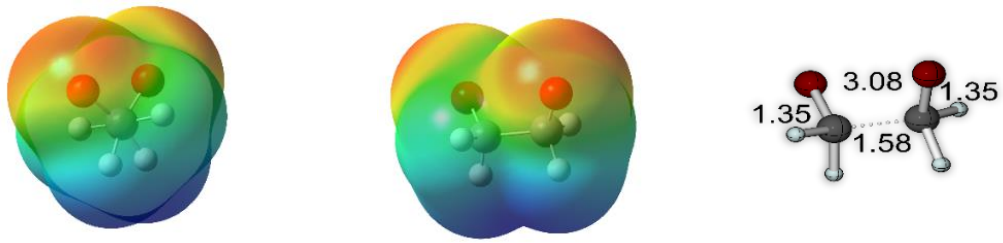

Figure 49. 1,2-Dioxetane TSS uB3LYP/6-31G(d). Electrostatic potential map and stationary point geometry. Isovalue -4.00e-2 to 4.00e-2. Distances in angstroms.

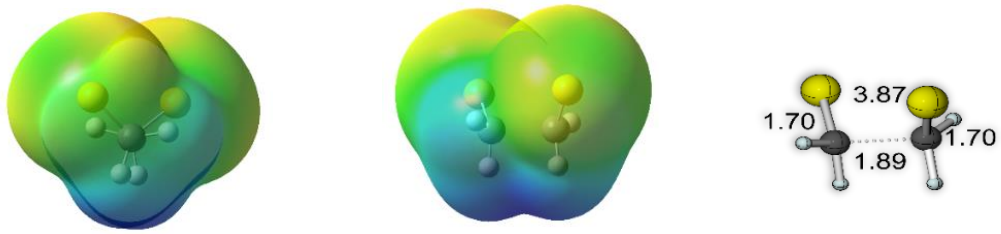

Figure 50. 1,2-Dithietane TSS uB3LYP/6-31G(d). Electrostatic potential map and stationary point geometry. Isovalue -4.00e-2 to 4.00e-2. Distances in angstroms.

Formation of the oxygen containing intermediate analogs 1,2-dioxetane and 1,3-dioxetane is endergonic resulting in formation of less stable (higher energy) products than

their respective reactants. Formation of the non-oxygen containing intermediate analogs is exergonic resulting in formation of more stable (lower energy) products than their respective reactants. 1,2-dithietane and 1,3-dithietane were the lowest and second lowest energy products in regards to their starting reactants, with cyclobutane in-between the energetic stability of the oxygen and sulfur containing intermediate analogs. Figures 51 and 52 depict the geometry and electrostatic potential map of the intermediate analogs ordered from left to right by least energetically stable to most energetically stable.

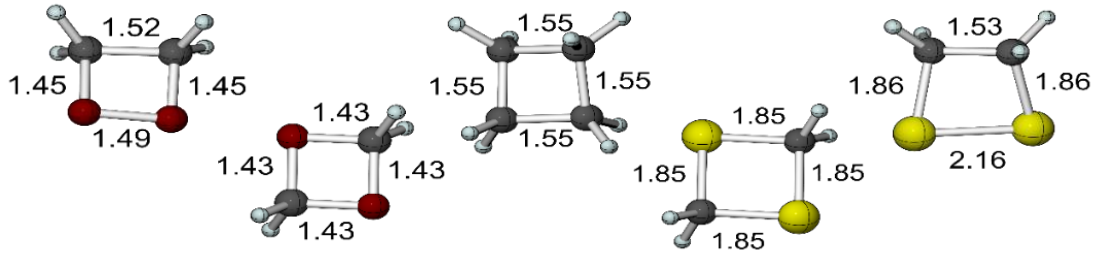

Figure 51. Intermediate analog stationary point minima geometries, uB3LYP/6-31G(d). Left to right cyclobutane, 1,3-dioxetane, 1,2-dioxetane, 1,3-dithietane, 1,2-dithietane. Distances in angstroms.

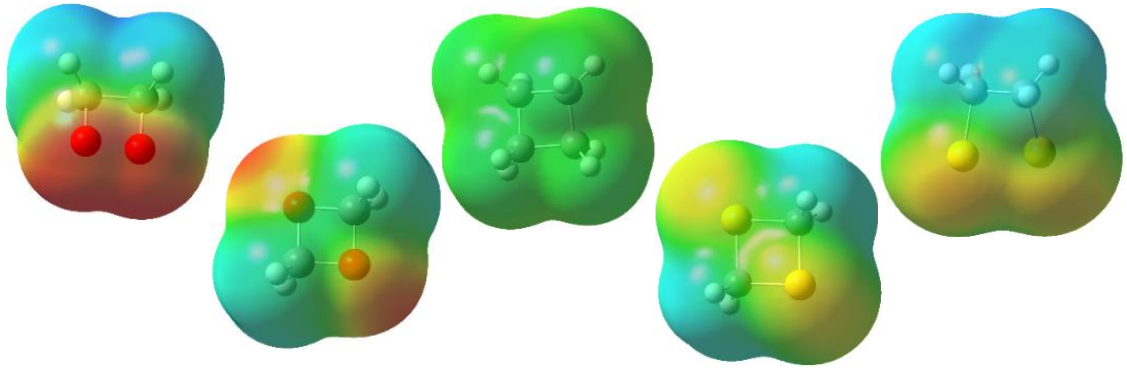

Figure 52. Intermediate analog stationary point minima electrostatic potential map, uB3LYP/6-31G(d). Left to right cyclobutane, 1,3-dioxetane, 1,2-dioxetane, 1,3-dithietane, 1,2-dithietane. Isovalue -4.00e-2 to 4.00e-2.

The gap in energy between each analog substantially decreases going from left to right as measured in kcal/mol with regard to each intermediates, starting reactants (Intermediate energy: 54.7, 5.4, -18.4, -21.9, -23.3; difference in energy: 49.9, 23.8, 3.5, 1.4)

Figures 53-55 depict a stepwise formation of intermediate analog 1,2-dithietane calculated using an unrestricted density functional theory model chemistry of uB3LYP/6-31G(d). The TSSs and connecting energy minimum displayed in Figure 53 are triplets. The reactant and product energies displayed in Figure 53 correspond to the singlet geometry energies.

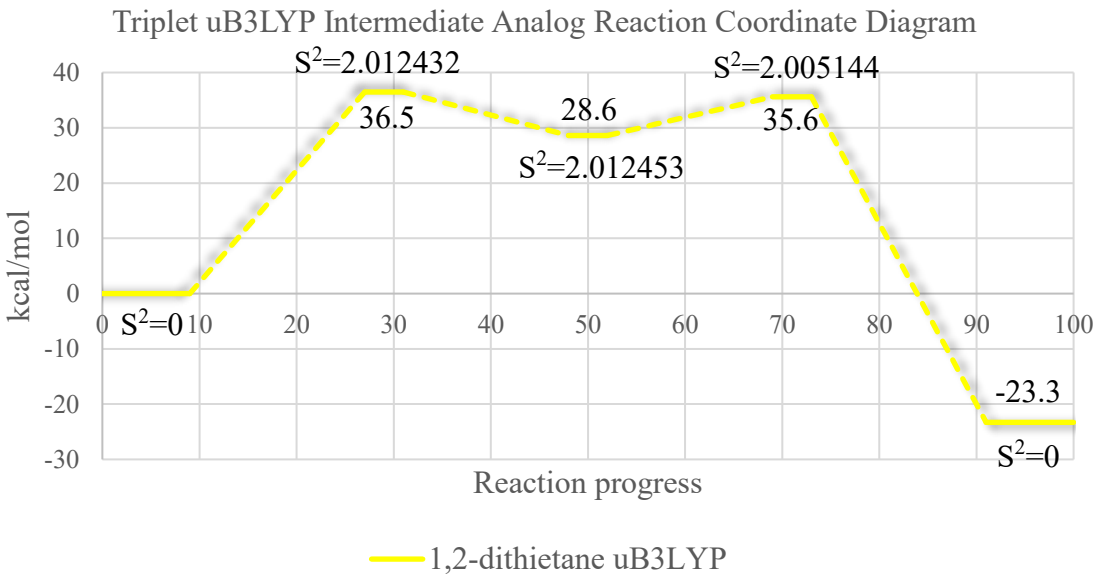

Figure 53. Reaction coordinate diagram for stepwise formation of intermediate analog 1,2-dithietane. TSSs 1 and 2 as well as the connecting energy minimum were computed in a triplet state. Reactant and product are shown in the relaxed singlet state.

The second triplet energy minimum following the second triplet TSS was optimized from the triplet geometry to the singlet 1,2-dithietane structure. Optimization of the first triplet TSS in the reverse direction from the last point of the triplet IRC failed to converge on a minimum. The last point of the IRC in the reverse direction as compared to the last point of the IRC in the forward direction showed the sulfur-sulfur bond distance lengthening, reaching 2.99 angstroms. Additionally, the last step in which the triplet energy minimum optimization failed SCF convergence the sulfur-sulfur distance had grown to 3.13

angstroms. Optimization of both the last point in the triplet IRC and triplet energy minimum optimization converged on a fully dissociated singlet energy minimum.

The first TSS asymmetrically forms a disulfide bond. The second TSS connects energy minima in which the first minimum structure has a disulfide bond and unpaired triplet electrons on both carbons. The second energy minimum structure has a carbon-carbon bond and unpaired triplet electrons on the two sulfur atoms. When the second triplet energy minimum is then optimized to a singlet it converges on the closed shell singlet 1,2-dithietane intermediate analog. All of the S^2 values are well with in the 10% limit of their spin expectation values meaning that they are all chemically meaningful structures.

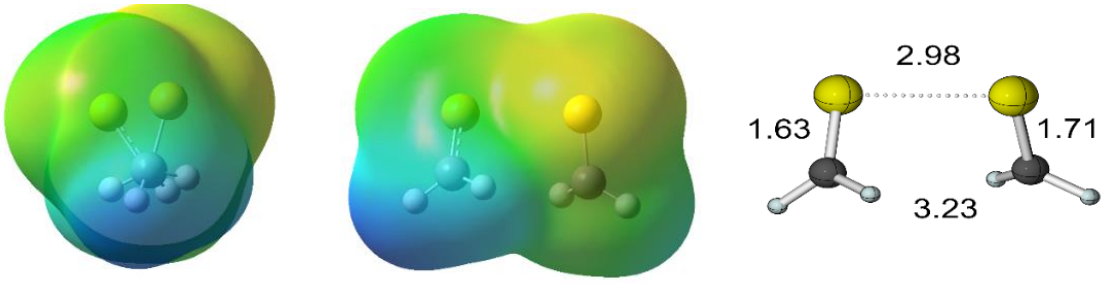

Figure 54. 1,2-Dithietane TSS1 uB3LYP/6-31G(d). Electrostatic potential map and stationary point geometry. Isovalue -4.00e-2 to 4.00e-2. Distances in angstroms.

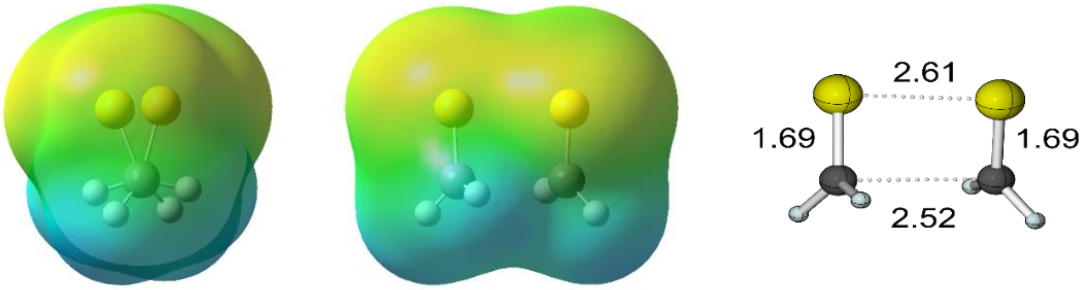

Figure 55. 1,2-Dithietane TSS2 uB3LYP/6-31G(d). Electrostatic potential map and stationary point geometry. Isovalue -4.00e-2 to 4.00e-2. Distances in angstroms.

Sulfur Extrusion

Figures 56-65 depict the first of the two proposed sulfur extrusion pathways ultimately yielding ethylene and diatomic sulfur starting from a 1,2-dithietane intermediate analog using a restricted density functional theory model chemistry of B3LYP/6-31G(d). This sulfur extrusion pathway is mirrored by a pathway starting from the oxygen containing intermediate analog 1,2-dioxetane using both a restricted and unrestricted density functional theory model chemistry of B3LYP/6-31G(d) and uB3LYP/6-31G(d).

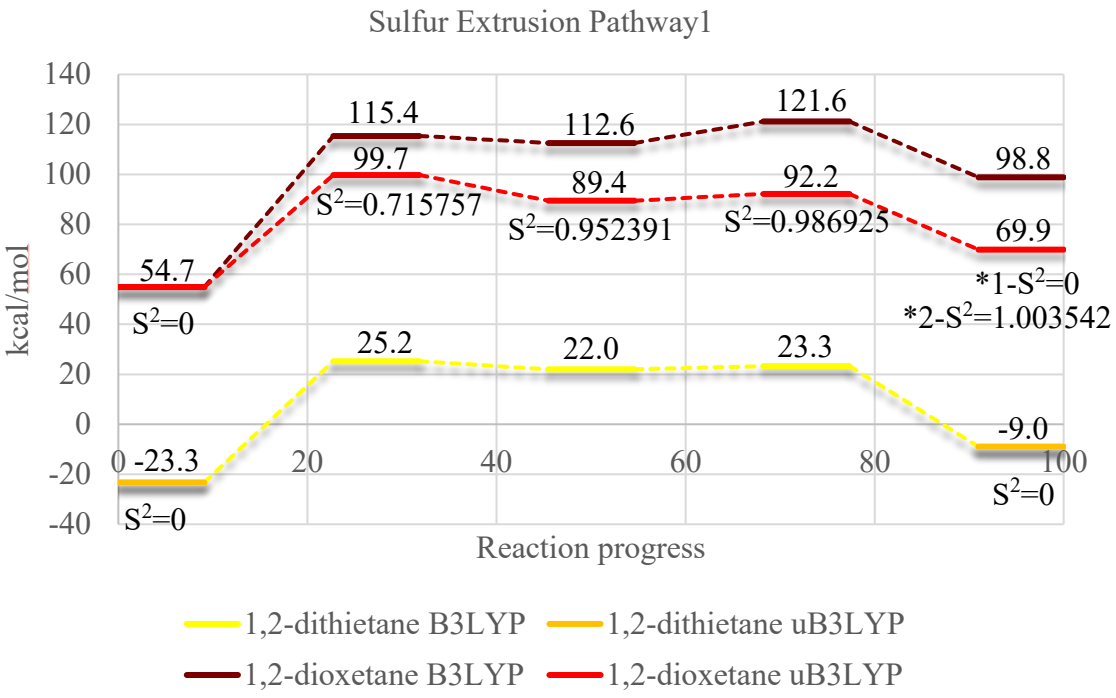

Figure 56. Reaction coordinate diagram of a two-step ionic bond cleavage pathway, resulting in sulfur extrusion, starting with 1,2-dithietane. This sulfur extrusion pathway is mirrored by similar pathways for 1,2-dioxetane using both restricted and unrestricted DFT.

The pathway for both 1,2-dithietane and –dioxetane intermediates progress through two similar transition states. In all three pathways, the first and second TSSs correspond to

sequential cleavage of the two σ-bonds between carbon-sulfur and carbon-oxygen atoms. The restricted calculations enforce double occupation of electrons in orbitals, making the mechanism ionic. A cation is formed on the carbon and anion on the sulfur or oxygen atom in the first TSS.

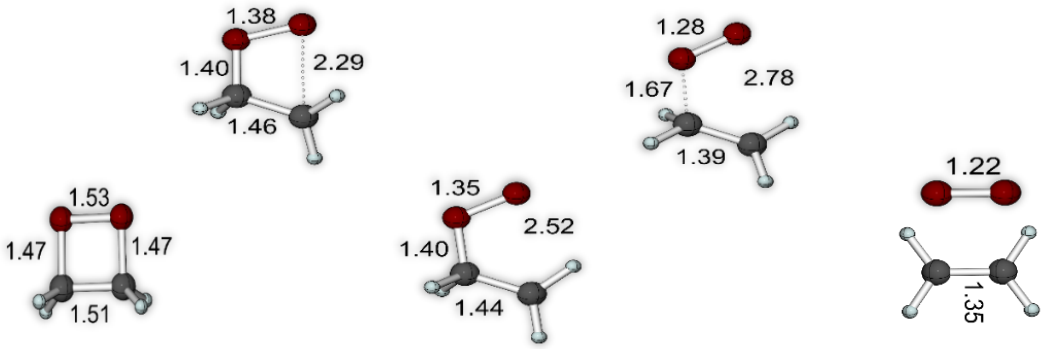

Figure 57. Extrusion Pathway 1. 1,2-dioxetane B3LYP/6-31G(d) stationary point geometries. Top row are transition states structures. Bottom row are minima. Distances in angstroms.

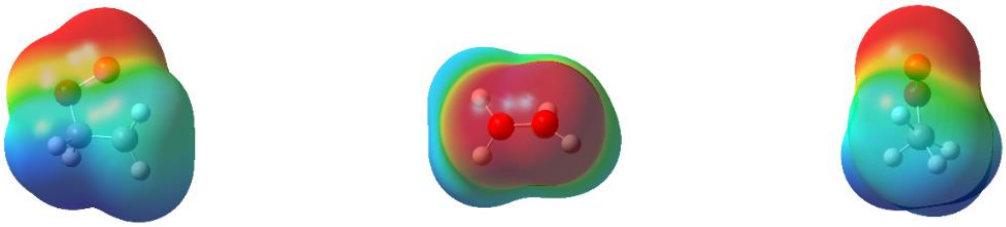

Figure 58. 1,2-Dioxetane TSS1 B3LYP/6-31G(d). Electrostatic potential map. Isovalue -4.00e-2 to 4.00e-2.

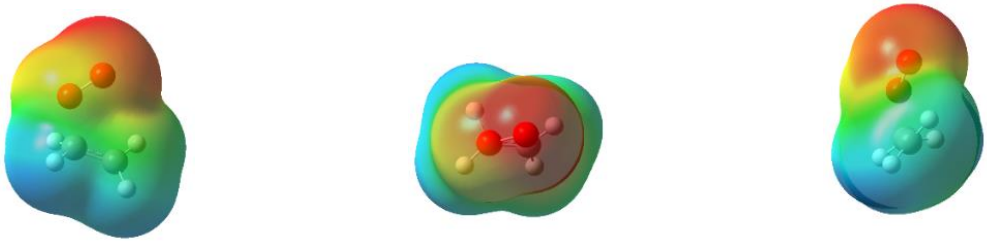

Figure 59. 1,2-Dioxetane TSS2 B3LYP/6-31G(d). Electrostatic potential map. Isovalue -4.00e-2 to 4.00e-2.

The unrestricted calculations all contained significant spin contamination from higher order spin states. The differences in energy between three pathways is reflected in the distribution of electron density seen in the electrostatic potential maps with the restricted 1,2-dioxetane calculation having the greatest separation in charge and the restricted 1,2-dioxetane calculation showing the least separation of charge.

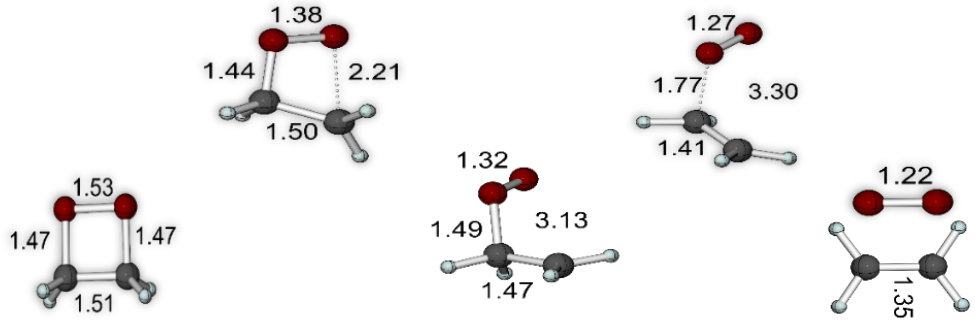

Figure 60. Extrusion Pathway 1. 1,2-dioxetane uB3LYP/6-31G(d) stationary point geometries. Top row are transition states structures. Bottom row are minima. Distances in angstroms.

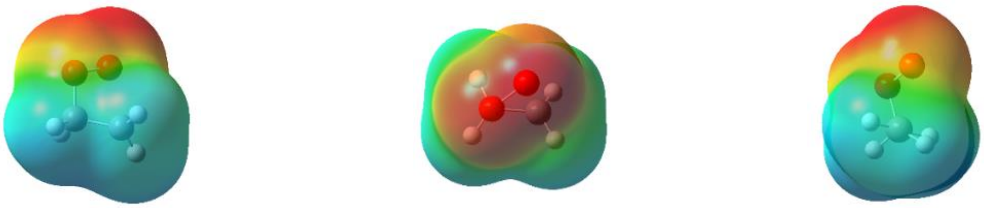

Figure 61. 1,2-Dioxetane TSS1 uB3LYP/6-31G(d). Electrostatic potential map. Isovalue -4.00e-2 to 4.00e-2.

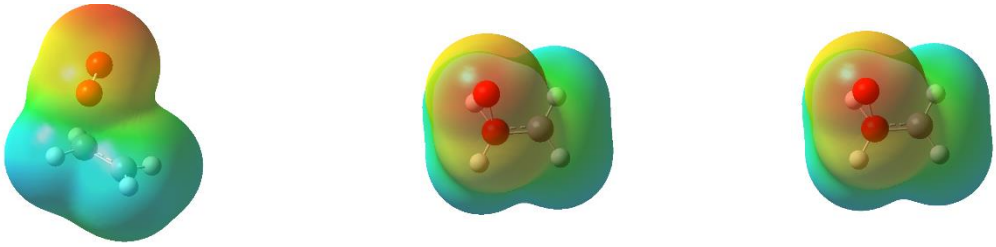

Figure 62. 1,2-Dioxetane TSS2 uB3LYP/6-31G(d). Electrostatic potential map. Isovalue -4.00e-2 to 4.00e-2.

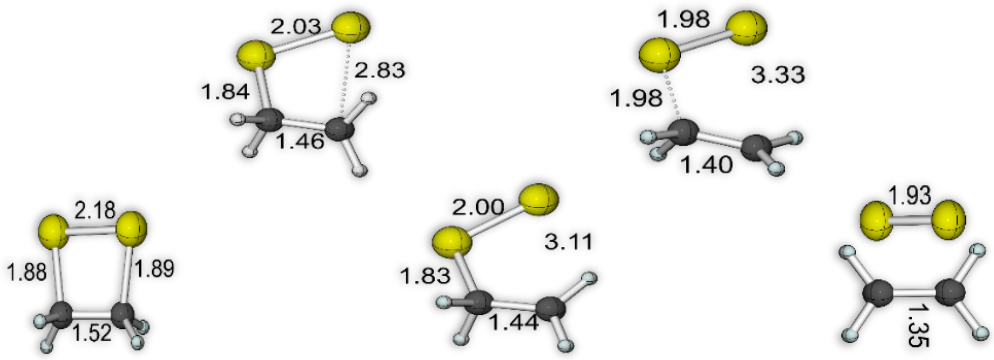

Figure 63. Extrusion Pathway 1. 1,2-dithietane B3LYP/6-31G(d) stationary point geometries. Top row are transition state structures. Bottom row are minima. Distances in angstroms.

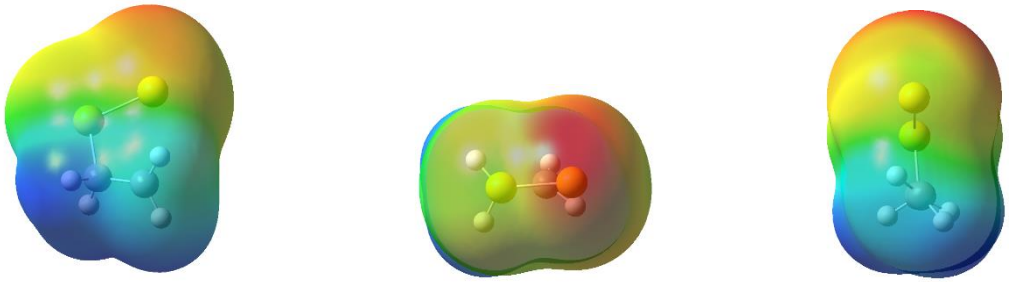

Figure 64. 1,2-Dithietane TSS1 B3LYP/6-31G(d). Electrostatic potential map. Isovalue -4.00e-2 to 4.00e-2.

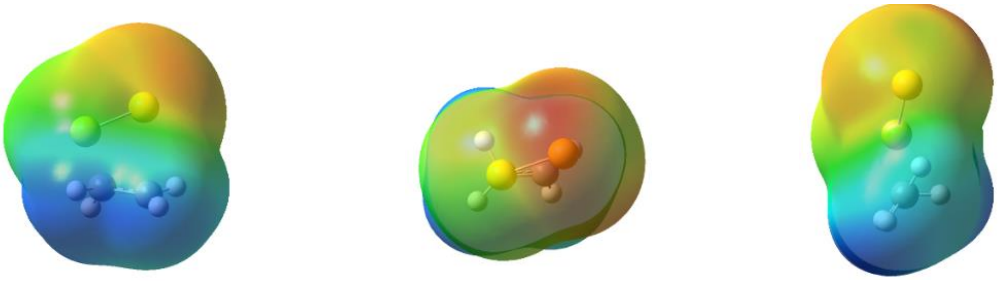

Figure 65. 1,2-Dithietane TSS2 B3LYP/6-31G(d). Electrostatic potential map. Isovalue -4.00e-2 to 4.00e-2.

Figures 66-75 depict the second proposed sulfur extrusion pathway ultimately yielding ethylene and diatomic sulfur starting from a 1,2-dithietane intermediate analog using a restricted and unrestricted density functional theory model chemistry of B3LYP/6-31G(d) and uB3LYP/6-31G(d). The same pathway is also calculated using

(8,8)-CASSCF. This sulfur extrusion pathway is, as before, mirrored by a pathway starting from the analogous oxygen-containing intermediate analog 1,2-dioxetane using both a restricted and unrestricted density functional theory model chemistry.

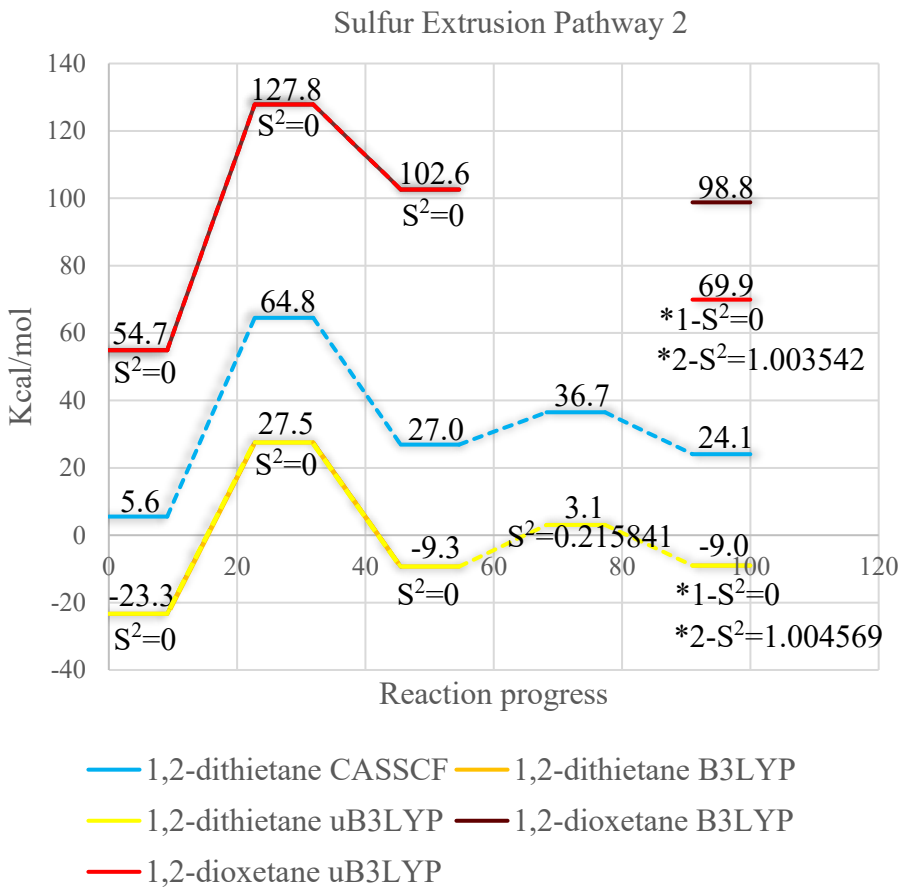

Figure 66. Reaction coordinate diagram of the second proposed sulfur extrusion pathway. Starting with 1,2-dithietane then undergoing concerted rearrangement followed by extrusion using both restricted and unrestricted DFT as well as (8,8)-CASCF. Sulfur extrusion is mirrored by similar pathways for 1,2-dioxetane using both restricted and unrestricted DFT.

This second proposed sulfur extrusion pathway also goes through two transition states. In the first transition state 1,2-dithietane and 1,2-dioxetane rearrange to a thiirane/oxirane structure with the second sulfur/oxygen atom attached to the heterocyclic atom of their

corresponding three membered ring. The S^2 values for all of the unrestricted calculations of the first transition state were exactly zero meaning they yielded identical structures to the restricted calculations. The rearrangement of the first transition state is then followed by ring collapse as diatomic sulfur separates from ethylene.

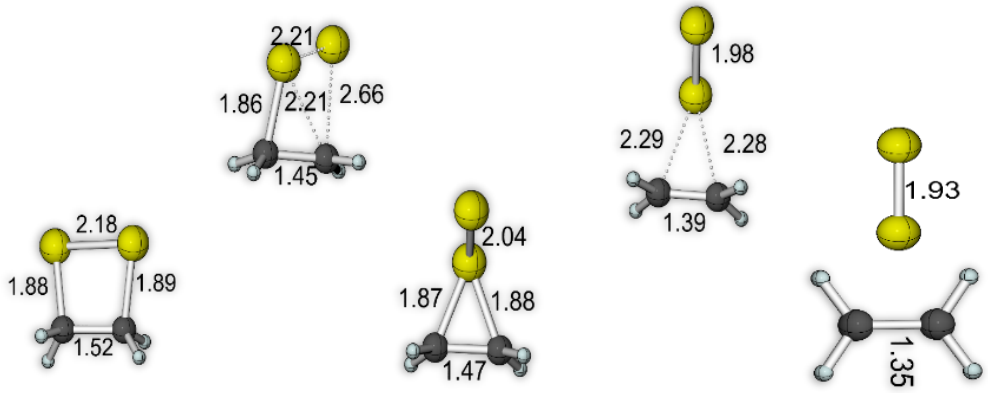

Figure 67. Extrusion Pathway 2. 1,2-dithietane CASSCF/6-31G(d) stationary point geometries. Top row are transition state structures. Bottom row are minima. Distances in angstroms.

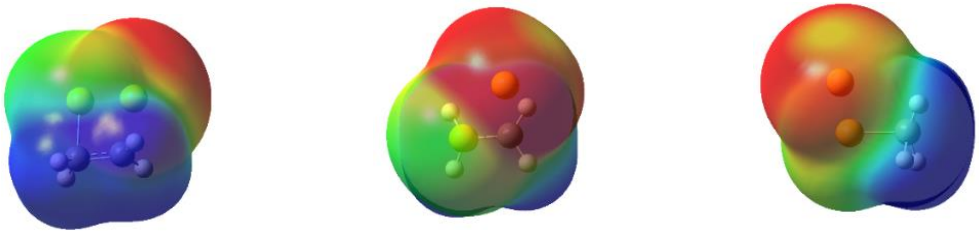

Figure 68. 1,2-Dithietane TSS1 CASSCF/6-31G(d). Electrostatic potential map. Isovalue -4.00e-2 to 4.00e-2.

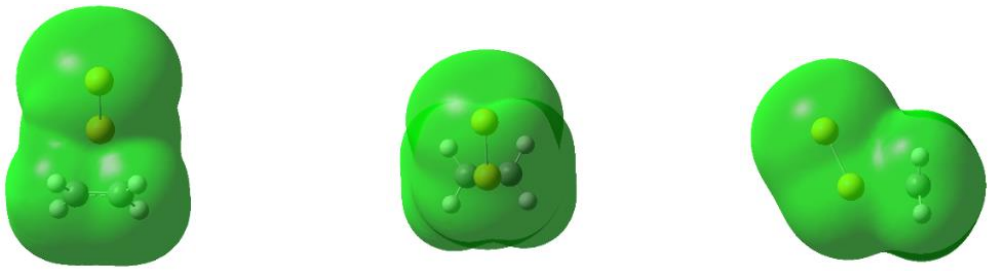

Figure 69. 1,2-Dithietane TSS2 CASSCF/6-31G(d). Electrostatic potential map. Isovalue -4.00e-2 t4.00e-2.

Oddly the second transition state by CASSCF yielded an electrostatic potential map of even electron distribution despite the fact that its corresponding stationary point geometry has the diatomic sulfur closer to the ethylene portion by 2.29 and 2.28 angstroms in the CASSCF calculation and 2.45 angstroms in the uB3LYP calculation.

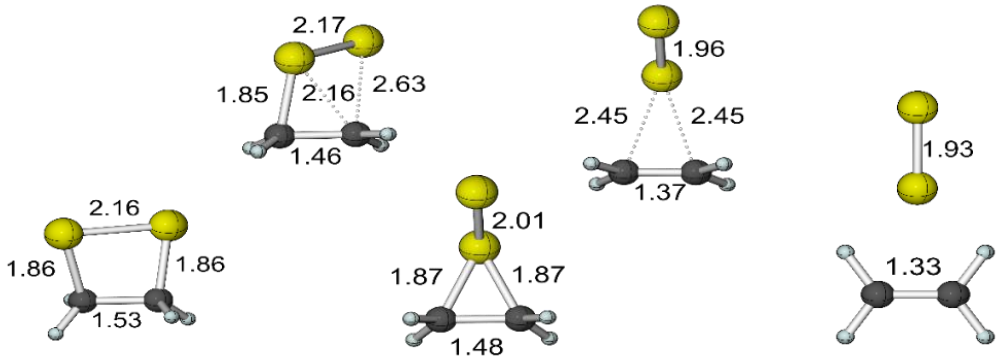

Figure 70. Extrusion Pathway 2. 1,2-dithietane uB3LYP/6-31G(d) stationary point geometries. Top row are transition state structures. Bottom row are minima. Distances in angstroms.

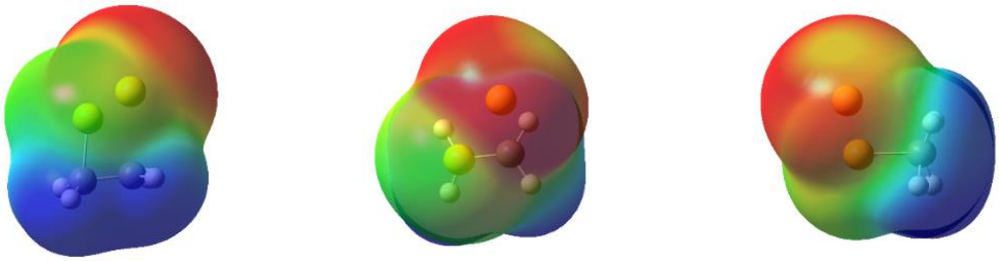

Figure 71. 1,2-Dithietane TSS1 uB3LYP/6-31G(d). Electrostatic potential map. Isovalue -4.00e-2 to 4.00e-2.

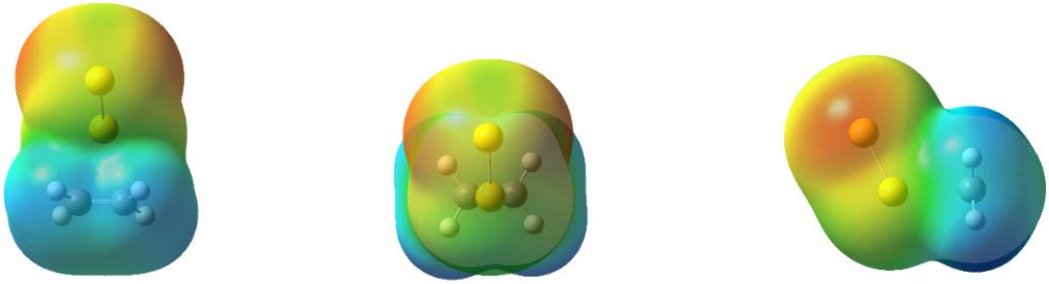

Figure 72. 1,2-Dithietane TSS2 uB3LYP/6-31G(d). Electrostatic potential map. Isovalue -4.00e-2 to 4.00e-2.

The second TSS was found using the computational method CASSCF and uB3LYP for 1,2-dithietane. The second transition state was not found for 1,2-dioxetane nor with restricted B3LYP for 1,2-dithietane.

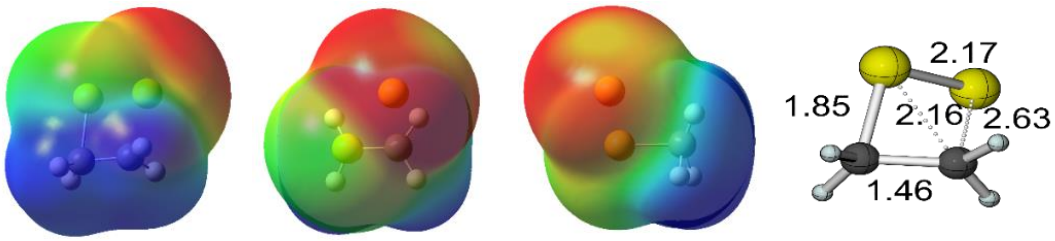

Figure 73. Extrusion Pathway 2. 1,2-dithietane B3LYP/6-31G(d). Electrostatic potential map and stationary point geometry. Isovalue -4.00e-2 to 4.00e-2. Distances in angstroms.

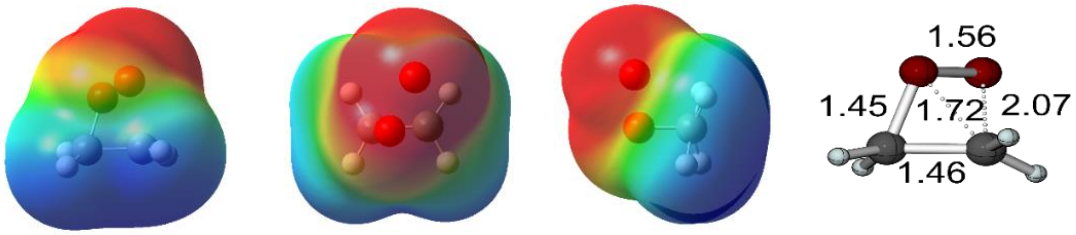

Figure 74. Extrusion Pathway 2. 1,2-dioxetane uB3LYP/6-31G(d). Electrostatic potential map and stationary point geometry. Isovalue -4.00e-2 to 4.00e-2. Distances in angstroms.

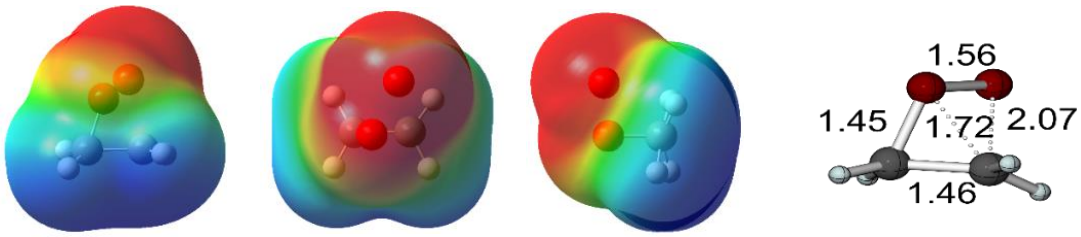

Figure 75. Extrusion Pathway 2. 1,2-dioxetane B3LYP/6-31G(d). Electrostatic potential map and stationary point geometry. Isovalue -4.00e-2 to 4.00e-2. Distances in angstroms.

CHAPTER 6: SUMMARY, CONCLUSION AND FUTURE DIRECTIONS

Summary

The CASSCF calculations consistently yielded substantially higher energy values than the DFT calculations. Using the example of the second sulfur extrusion pathway the following two tables detail the difference in energy values obtained from CASSCF versus DFT. The coefficient of variance shows that the relative difference in energy between equivalent structures obtained with CASSCF versus DFT is less than the relative difference in energy of the reaction barriers obtained with CASSCF versus DFT. However, the average difference in reaction barrier height was only 3.15 kcal/mol.

Table 1. Comparison of energies values obtained by CASSCF versus DFT for equivalent energy minimum structures (MS) and transition state structures (TSS) for sulfur extrusion pathway 2.

(kcal/mol)	CASSCF	DFT	Absolute Difference	Average Difference
MS1	5.6	-23.3	28.9	33.8
TSS1	64.8	27.5	37.3	Standard Deviation
MS2	27.0	-9.3	36.3	2.93
TSS2	36.7	3.1	33.6	Coefficient of Variance
MS3	24.1	-9.0	33.1	0.087

Table 2. Comparison of energies values obtained by CASSCF versus DFT for the difference in energy barriers separating equivalent energy minimum structures (MS) and transition state structures (TSS) for sulfur extrusion pathway 2.

(kca/mol)	CASSCF	DFT	Absolute Difference	Average Difference
MS1-TSS1	59.2	50.8	8.4	3.15
TSS1-MS2	37.8	36.8	1	Standard Deviation
MS2-TSS2	9.7	12.4	2.7	3.14
TSS2-MS3	12.6	12.1	0.5	Coefficient of Variance
				0.996

The following reported energies were obtained using the DFT functional B3LYP or uB3LYP with a 6-31G(d) basis set. Of the five intermediate analogs investigated, formation of the oxygen containing intermediate analogs 1,2-dioxetane and 1,3-dioxetane were endergonic at a zero-point corrected energy of 54.7 kcal/mol and 5.4 kcal/mol relative to reactants. Formation of cyclobutane and the two sulfur containing intermediate analogs 1,2-dithietane and 1,3-dithietane were exergonic at a zero-point corrected energy of -18.4 kcal/mol, -21.9 kcal/mol and -23.3 kcal/mol relative to reactants.

Across the board, all transition state structures leading to 1,2-dithietane and 1,3-dithietane were lower than that of the 1,2-dioxetane and 1,3-dioxetane intermediates. The highest energy transition state structure leading to a sulfur containing intermediate was the unrestricted stepwise triplet DFT 1,2-dithietane rate limiting transition state at 36.5 kcal/mol and the lowest energy oxygen containing transition state was the restricted DFT 1,3-dioextane [2+2] supra-supra transition state at 43.8 kcal/mol.

The two sulfur extrusion pathways have similar energetic barriers at their rate limiting steps differing by 2.5 kcal/mol. The first sulfur extrusion pathway's largest energetic barrier was 48.5 kcal/mol. The second sulfur extrusion pathway's largest energetic barrier was 50.8 kcal/mol

Historically, the unimolecular thermal decomposition of cyclobutane to two equivalents of ethylene and reverse reaction of ethylene dimerizing to form cyclobutane has been the subject of much debate over whether the reaction is governed by a stepwise diradical mechanism or a concerted supra-antara [2+2] cycloaddition.[66] Literature values list an activation energy of 62 kcal/mol for the thermal decomposition of cyclobutane and 44 kcal/mol for its formation.[66,67] This is in close agreement with the unrestricted DFT

stepwise calculation with a peak activation energy of 40.9 kcal/mol for the first transition state with the other two transition states ~2 kcal/mol lower than the first. The difference in energy between the first transition state and cyclobutane was 59.3 kcal/mol.

The thermal decomposition of 1,2-dioxetanes has historically also been the subject of much debate between whether it occurs by a concerted mechanism proposed by Turro or a stepwise biradical mechanism proposed by Richardson.[24,26] The unrestricted supra-supra 1,2-dioxetane TSS came the closest to the literature activation energy value of 24 kcal/mol at 29.7 kcal/mol. Computational analysis of the thermal decomposition of 1,2-dioxetane by Luca De Vico et al. using CASPT2 supports a biradical mechanism in which the oxygen-oxygen bond cleaves first forming a diradical.[33] The diradical can exist in a singlet state, and excited singlet state or a triplet state with intersecting potential energy surfaces. This is reflected in the spin contamination values all hovering around one seen in both the 1,2-dioxetane transition states and the 1,2-dithietane unrestricted DFT [2+2] supra-supra transition state. Unfortunately, attempts at finding an unrestricted stepwise pathway are currently held up in SCF purgatory.

Conclusion

These results suggest that the reaction proceeds through a sulfur-containing intermediate. Both 1,2-dithietane and 1,3-dithietane are of similar energetic stability differing by only 1.4 kcal/mol in favor of 1,2-dithietane. Furthermore the π-stacking of the benzene dimer is calculated to have a binding energy of 2-3 kcal/mol and the 1,2-

dithietane due to its structure likely may benefit from π-stacking, too, further stabilizing it as an intermediate.[68]

While most of the unrestricted calculations containing significant spin contamination (more than 10% of the expected value) do not correspond to physically meaningful chemical structures, they do however hint at the proximity in energy of the potential energy surfaces of higher spin states, due to the unrestricted variational freedom of α and β orbitals. The most likely spin state contamination for a molecule specified as a singlet is a triplet, which is consistent with a calculated total spin value near 1.[29,65] Correspondingly as sulfur and oxygen are both chalcogens, 1,2-dithietane may have similar chemistry as 1,2-dioxetane with regard to intersecting potential energy surfaces of singlet and triplet states. The spin contamination in S^2 values seen in the 1,2-dithietane [2+2] supra-supra transition state (S^2=0.98202) is very similar to that of 1,2-dioxetane [2+2] supra-supra transition state (S^2=1.005537). Subsequent rerunning of the concerted 1,2-dithietane unrestricted DFT [2+2] supra-supra transition state as a triplet with a spin multiplicity of 3 yielded the second transition state in the stepwise triplet formation of 1,2-dithietane. The singlet and triplet transition state structures are similar in energy at 35.8 to 35.6 kcal/mol a 0.8 kcal/mol difference. Most importantly the triplet transition state has an S^2 value of 2.005144 handily within the 10% spin contamination limit of what would be expected for a triplet making it a physically meaningful chemical structure and representing a viable pathway for formation of the 1,2-dithietane intermediate analog. These findings of the intermediate analog formation are consistent with the one-pot one-step bifluorenylidene microwave assisted synthesis protocol. A study by Rodriguez et al. on the influence of polarity in microwave assisted organic synthesis

(MAOS) predicts that reactants with polar functional groups forming more stable products can readily occur at over 30 kcal/mol.[69] An example given was a Diels-Alder cycloaddition with an activation energy of 41.8 kcal/mol that was ran as a MAOS for 3 min and resulted in a 78% yield.

The rate-limiting step of both sulfur extrusion pathways 1 and 2 are ionic and both lead to an energy minimum with formal positive and negative charges as seen in Figure 72. The first transition state of pathway 1 forms an anion on the sulfur atom after bond cleavage and a cation on the carbon atom. The empirical system contains polycyclic aromatic substructures not present in our analog systems. Formation of a carbocation on one of the two fluorenylidene substructures would make it anti-aromatic on that portion of the structure as seen in Figure 76 and thus result in an unfavorable energetic barrier. Sulfur extrusion pathway 2 does not have this concern as it proceeds through a rearrangement forming a three membered ring between the two fluorenylidene substructures.

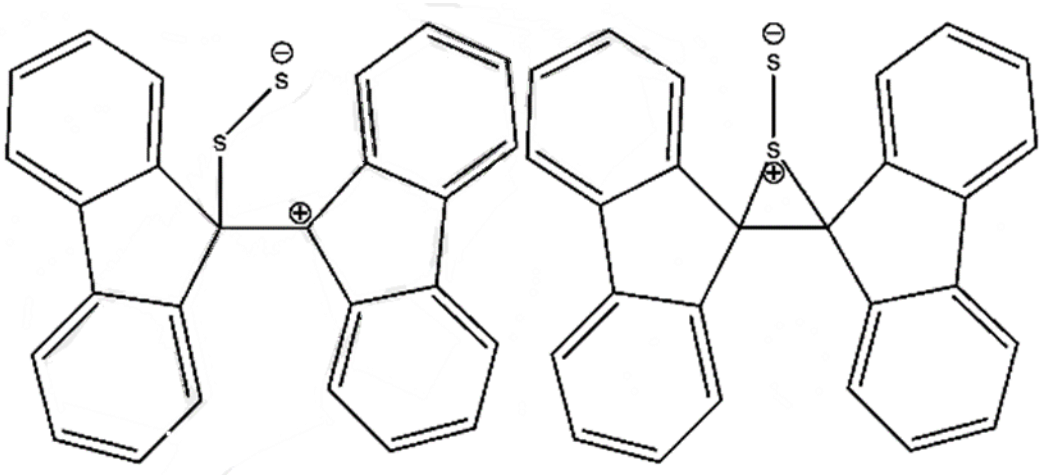

Figure 76. Energy minima following the rate limiting step of sulfur extrusion pathways 1 and 2. The structure on the left corresponding to pathway 1 and the structure on the right to pathway 2.

I propose that that the percent yield of the reaction would be improved by electron donating substituents such as an amine.* This could help stabilize the anti-aromaticity of the one fluorenylidene substructure in extrusion pathway 1. This could also lower the energetic barriers of extrusion pathway 2 by reducing the formal positive charge of the sulfur in the three-membered ring via induction. Figure 77 shows bifluorenylidenes reported in the literature following a Lawesson's reagent mediated synthesis starting from a fluorenone scaffold.

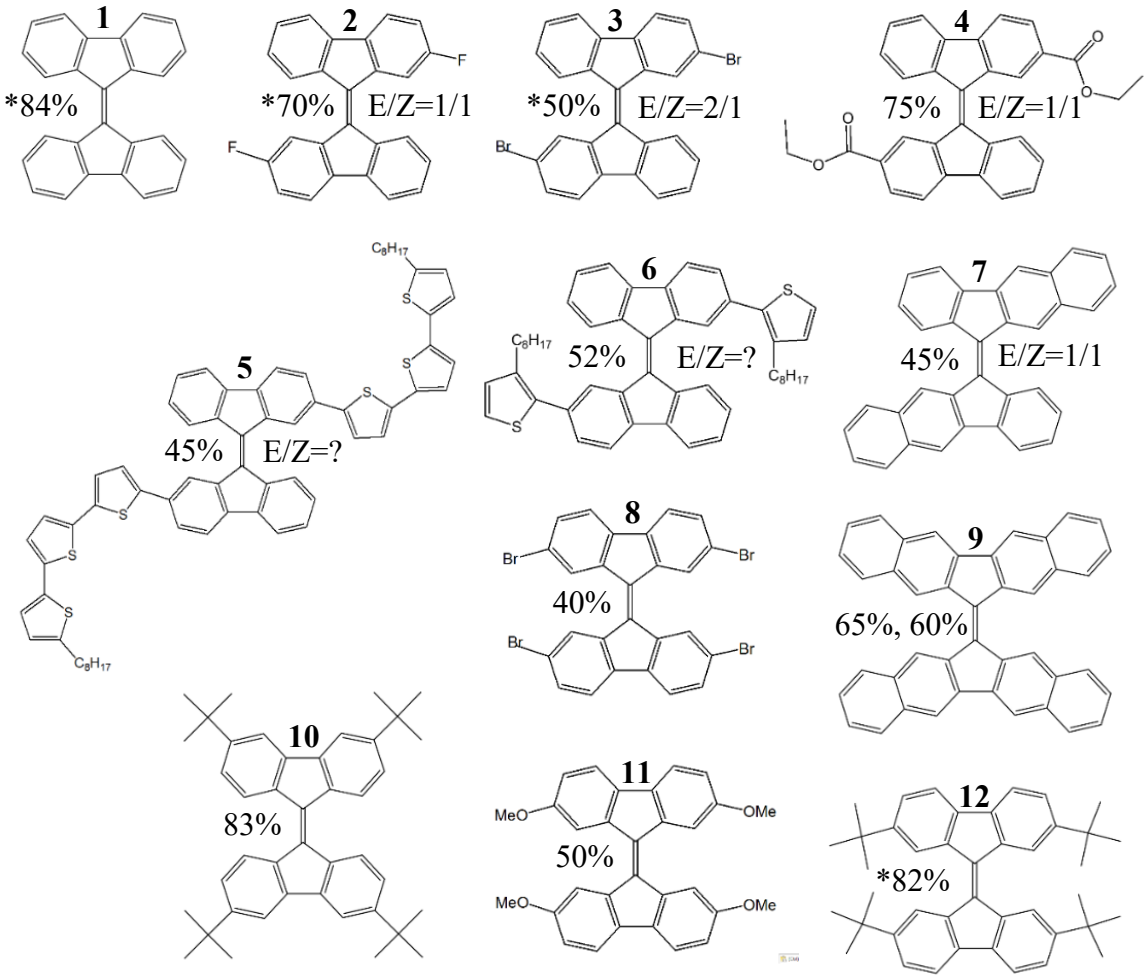

Figure 77. Lawesson's reagent mediated syntheses starting from a fluorenone scaffold in literature. Asterisk indicates microwave assisted synthesis and not refluxed.[16,37,70,71,72]
*this argument assumes that either: 1) Rxn is kinetically controlled and barrier is nearly insurmountable, and 2) There is no side product.

Many factors complicate evaluating results from the literature reported syntheses because the reaction conditions varied extensively. Some were microwave assisted syntheses and others were refluxed. The microwave assisted syntheses (MAS) were solventless, whereas the refluxed reaction mixtures used primarily toluene or benzene. Products **4** and **10** were solventless and heated by sand bath till melted. Despite this, four significant insights can be gleaned that support the formation of a (2,2) cycloadduct 1,2,-intermediate: effect of electron donating/withdrawing substituents, π-stacking, E/Z isomer ratio and steric repulsion.

Following along with Figure 77, products **2** and **3** had yields lower than **1** and **12** despite all four following a similar MAS procedure. **2** and **3** have electron withdrawing halogen substituents, whereas **1** has no substituents and **12** has four very bulky tert-butyl substituents. The steric effect of a tert-butyl substituent can be quantified with an A-Value.[73] Tert-butyl has an A-Value of 2, bromine has an A-Value of 0.38, fluorine has an A-value of 0.15 and deuterium has an A-Value of 0.006. The larger and more sterically hindering a substituent is the larger it's A-Value. By argument of steric hindrance, **12** should have the lowest yield of the four yet it has the second highest. I argue that is the case because, although it would cause significant steric repulsion in the 1,2-dithietane intermediate structure, tert-butyl groups are moderately electron donating due to hyperconjugation.[74] Thus, supporting the two proposed sulfur extrusion pathways. **2** has a higher yield than **3** even though it is more electron withdrawing than **3**. However, **3** is electron withdrawing and significantly more sterically hindering and will additionally have greater issues with electrostatic repulsion not faced by tert-butyl substituents. This is further evidenced by the fact that the E/Z isomers are formed in a 1/1 ratio for **2** but in a

2/1 ratio for **3**. Thus supporting a 1,2-intermediate structure as steric repulsion would play a much bigger role than in a 1,3-intermediate. Refer to Figure 19 chapter 3 to help visualize this.

4 and **10** had similar syntheses, both were heated with a sand bath in a solventless reaction mixture till melted. **10** has a higher yield than **4** despite the fact that **10** is more sterically hindered as it's four tert-butyl substituents have an A-value of 2 compared to the two CO_2Et substituents of **4** with an A-value of 1.2 because tert-butyl substituents are electron donating as opposed the electron withdrawing ester groups of product **4**.

Products **7**, **8**, **9** and **11** had similar syntheses, refluxed in either boiling toluene or benzene. **9** had the highest yield fitting the proposed sulfur extrusion pathways as it would not have had any issues with sterically repulsive substituents but would benefit from increased π-stacking, as well as increased conjugation from a larger aromatic ring system. **8** had the lowest yield due to it's four sterically hindering and electrostatically repulsive bromine substituents which additionally are electron withdrawing further lowering its yield in accord with the proposed pathways. **11** had the second highest yield as it had four strongly electron donating methoxy substituents. However, methoxy substituents have an A-value of 1.2 and due to the oxygens would further create electrostatic repulsion between the two fluorenylidene moieties of the 1,2-dithietane intermediate causing it to have a lower yield than **9**. **7** had a yield higher than that of **8** but lower than **11** because while it didn't have any of the steric or electrostatic repulsion of **11** repulsion it also did not have **4** strongly electron donating substituents. While **9** had a higher yield than **11** and **7** has a similar aromatic ring system to **9** the smaller aromatic

ring system of **7** relative to **9** would mean less conjugation and less π-stacking and thus **9** has a smaller yield than **11**.

5 and **6** were both synthesized by the same reflux procedure and both have thiophene substituents, which increase the conjugation of the fluorenylidene moieties and are electron donating. **5** has oligothiophene substituents and a lower yield than **6** indicating that the steric repulsion played a more important role in this case. Unfortunately, there is no E/Z ratio data on this as I suspect it would be heavily skewed towards favoring the E isomer for **5** relative to **6**. Reducing half of the productive angles of attack would certainly effect the reaction rate and provide an interesting bit of information in analyzing the most likely mechanism.

Future Directions

The CASSCF calculations yielded significantly higher energy calculations relative to the energies obtained using DFT for equivalent structures suggesting that there is a systematic error in how they were performed. One possibility may be that the fundamental assumption of combining the energy of two reactants using a (4,4) active space that's is half the size of the products (8,8) active space is not a valid comparison. Another possibility is to pursue implementing an MP2 energy correction keyword to the CASSCF calculations. It will be important for the future of this project as CASSCF allows one to perform an optimization to locate conical intersections, thus optimizing to the geometry at which different electronic states become degenerate.[29] These structures will then serve as the starting structures for CASPT2 calculations, which can more accurately describe the energy of excited states.[75]

Another important direction will be to take the transition state structures located with DFT for the analog systems and apply them to the full system. They will serve as a starting point for constructing jobs providing insights into specifying the initial geometries. Specifically, modeling the two sulfur extrusion pathways as they are as of yet better defined than the intermediate formation. It will be of key interest to see how the polycyclic aromatic rings effect the reaction barrier heights and if the first step of both extrusion pathways remains the rate limiting step in forming 9,9'-bifluorenylidene. Locating the transition state structures will likely be a much more difficult task than simply replacing the four hydrogens of 1,2-dithietane with fluorenylidene moieties, however locating energy minima is a relatively quick and easy task. An interesting mini side-project would be to find the energy minima for the fluorenthione scaffolds, 1,2- /1,3-intermediates and substituted 9,9'-bifluorenylidene products published in the literature and see if the calculated energetic stabilities correlate with the published percent yields.

Furthermore, it would be insightful to run a series of wet-lab syntheses mirrored computationally just as mentioned prior for the already published syntheses, in which Hammett values and A-values were used to make a systematic list of scaffolds for dimerization that show a clear and even gradation in their effect on the percent yield of formed bifluorenylidenes. A specific example being: does increasing A-Values of singly substituted fluorenylidene scaffolds increase the E to Z isomer ratio? Then after establishing trends for Hammett values and A-values on percent yield, mix and match them with additional characteristics to further parse possibilities for the inner workings of the mechanism, such as the possible role of π-stacking. Most importantly, these syntheses need to have standardized protocols not intended to maximize the percent yield but

instead to rigidly enforce consistency in manipulable variables such as reaction time and temperatures. Thereby allowing clearer visibility of the trends in percent yield as they relate to Hammett values and A-values. Finally, I would use time-dependent-DFT to calculate substituent effect on the HOMO and LUMO of 9,9'-bifluorenylidene using the same substituents as in the systematic wet-lab syntheses. The goal to be able to effectively correlate the empirical data in a way that is consistent with calculations and a complete mechanism of bifluorenylidenes synthesis. Because from this, the dream is to enable *a priori* rational design of high yield production for electron acceptors with finely tuned band gaps, from the comfort of an armchair.

REFERENCES

(1) Wiley Online Library. https://onlinelibrary.wiley.com/page/journal/10991395/homepage/ProductInformation.html (accessed Dec 21, 2017), Journal of Physical Organic Chemistry Overview.

(2) Tidwell, T.T. The First Century of Physical Organic Chemistry: A Prologue, 1997. International Union of Pure and Applied Chemistry. https://old.iupac.org/publications/pac/special/0297/tidwell.pdf (accessed Dec 21, 2017)

(3) Hammet, L.P. *Physical Organic Chemistry,*1; McGraw Hill: New York, NY, 1940.

(4) Knapman, K. Computational chemistry on the desktop PC. Chem. Innov. [Online] **2000**, 30, 10. http://pubs.acs.org/subscribe/archive/ci/30/i10/toc/toc_i10.html (accessed Dec 21, 2017)

(5) Nobel Prize. https://www.nobelprize.org/nobel_prizes/chemistry/laureates/1998 (accessed Dec 21, 2017), The Nobel Prize in Chemistry 1998, Walter Kohn, John Pople.

(6) American Chemical Society. https://www.acs.org/content/acs/en/careers/college-to-career/chemistry-careers/computational-chemistry.html (accessed Dec 21, 2017), Chemistry Careers, Computational Chemistry Overview.

(7) Eakins, G. Substituent and Conjugation Effects on the Homo-Lumo Bandgaps of 9-Fluorenones, 9-Fluorenylidenes, and Related Derivatives. Masters Thesis, Missouri State University, Springfield, MO, Summer 2010.

(8) Schleyer, P. Introduction: Aromaticity. *Chem. Rev*. **2001**, 101, 1115-117.

(9) Hoffmann, A. W. On insolinic acid. *Proc. R. Soc. Lond*. **1856**, 8, 1-3.

(10) Hückel, E. Quantentheoretische Beiträge zum Benzolproblem I. *Zeit. Phys*. **1931**, 70, 204-286.

(11) Hückel, E. Quantentheoretische Beiträge zum Benzolproblem II. *Zeit. Phys*. **1931**, 72, 310-337.

(12) Hückel, E. Quantentheoretische Beiträge zum Benzolproblem III. *Zeit. Phys*. **1931**, 70, 628-648.

(13) Doering, W. Abstracts of the American Chemical Society Meeting, September, 1951, New York, NY.

(14)Robert, J. D.; Streitwieser, A; Regan, C. M. Small-Ring Compounds. X. Molecular Orbital Calculations of Properties of Some Small-Ring Hydrocarbons and Free Radicals. *J. Am. Chem. Soc.* **1952**, 74 , 4579–4582.

(15)Bühl, M.; Hirsch, A. Spherical Aromaticity of Fullerenes. *Chem. Rev*. **2001**, 101, 1153-1184.

(16)Brunetti, F. G.; Gong, X.; Tong, M.; Heeger, A. J.; Wudl, F. Strain and Hückel Aromaticity: Driving Forces for a Promising New Generation of Electron Acceptors in Organic Electronics. *Ang. Chem*. **2010**, 49, 532-536.

(17)Cohen, Y.; Klein, J.; Rabinovitz, M. Stable polycyclic anions: dianions from overcrowded ethylenes. J. Chem. Soc., *Chem. Commun.* **1986**, 14, 1071-1073

(18)Grossman, R.B. *The Art of Writing Reasonable Organic Reaction Mechanisms,* 2; Springer: New York, NY, 2003.

(19)Hoffmann, R.; Woodward R. B. Selection Rules for Concerted Cycloaddition Reactions. *J. Am. Chem. Soc*. **1965**, 87, 2046-2048

(20)IUPAC. *Compendium of Chemical Terminology*, 2. Blackwell Scientific Publications, Oxford, 1997, Compiled by A. D. McNaught and A. Wilkinson.

(21)Kopecky, K. R.; Mumford, C. Luminescence in the thermal decomposition of 3,3,4-trimethyl-1,2-dioxetane *Can. J. Chem*. **1969**, 47, 709.

(22)Carpenter, B. K. Electronically nonadiabatic thermal reactions of organic molecules. *Chem. Soc. Rev*. **2006**, 35, 736-747

(23)Wilsey, S.; Bernardi, F.; Olivucci, M.; Robb, M. A.; Murphy, S.; Waldemar, Adam. The Thermal Decomposition of 1,2-Dioxetane Revisited. *J. Phys. Chem. A*. **1999**, 103, 1669-1677.

(24)Turro, N. J.; Devaquet, A. Chemiexcitation Mechanisms - Role of Symmetry and Spin-Orbit Coupling in Diradicals. *J. Am. Chem. Soc.* **1975**, 97, 3859−3862.

(25)O'Neal, H. E.; Richardson, W. H. Thermochemistry of 1,2- Dioxetane and Its Methylated Derivatives. Estimation of Activation Parameters. *J. Am. Chem. Soc.* **1970**, 92, 6553−6557.

(26)Richardson, W. H.; O'Neal, H. E. Thermochemistry and Estimated Activation Parameters for the Thermal Decomposition of 1,2-Dioxetanedione, 4-tert-Butyo-1,2-Dioxetane-3-One and 4,4-Dimethyl-1,2-Dioxetane-3-One. *J. Am. Chem. Soc.* **1972**, 94, 8665−8668.

(27)Farahani, P.; Baader, W. J. Unimolecular Decomposition Mechanism of 1,2-Dioxetanedione: Concerted or Biradical? That is the Question! *J. Phys. Chem. A.* **2017**, 121, 1189-1194.

(28)Schrödinger, E. An Undulatory Theory of the Mechanics of Atoms and Molecules. *Phys. Rev.* **1926**, 28, 1049-1070.

(29)Cramer, C. *Essentials of Computational Chemsitry Theories and Models*, 2; John Wiley & Sons: Chichester, England, 2004.

(30)Born, M.; Oppenheimer, J. R. Zur Quantentheorie der Molekeln. *Ann. Phy.* **1927**, 389, 457-484.

(31)Mcquarrie, D. A.; Simon, J. D. *Physical Chemistry A Molecular Approach*, 1; University Science Books: Sausilito, CA, 1997.

(32)Hammond, G. S. A Correlation of Reaction Rates. *J. Am. Chem. Soc*. **1955**, 77, 334–338.

(33)De Vico, L.; Liu, Y. J.; Krogh, J. W.; Lindh, R. Chemiluminescence of 1,2-Dioxetane. Reaction Mechanism Uncovered. *J. Phys. Chem. A* .**2007**, 111, 8013-8019.

(34)National Renewable Energy Laboratory. https://www.nrel.gov/workingwithus/re-photovoltaics.html (accessed Jan 10, 2017), Solar Photovoltaic Technology Basics.

(35)Kippelen, B.; Bredas, J-L. Organic Photovoltaics. *Energy Environ. Sci*. **2009**, 2, 251-261.

(36)Li, C.; Yip, H.; Jen, A. Functional fullerenes for organic photovoltaics. *J. Mat. Chem*. **2012**, 22, 4161-4177.

(37)Eakins, G.; Cooper, M.; Gerasimchuk, N.; Phillips, T.; Breyfogle, B.; Stearman, C. Structural influences impacting the role of the 9-ylidene bond in the electronic tuning of structures built upon 9-fluorenylidene scaffolds. *Can. J. Chem*. **2013**, 91, 1059-1071.

(38)Miessler, G. L. *Inorganic Chemistry*, 5th; Pearson: London, England, 2013.

(39)Fachetti, A. Polymer donor–polymer acceptor (all-polymer) solar cells. *Mater. Today*. **2013**, 16, 123-132.

(40)Al-Ibrahim, M.; Roth, H. K.; Zhokhavets, U.; Gobsch, G.; Sensfuss, S. Flexible large area polymer solar cells based on poly(3-hexylthiophene)/fullerene. *Energ. Mat. Sol. Cells.* **2005**, 85, 13-20.

(41)Sdfas Hoeben, F. J. M.; Jonkheijm, P.; Meijer, E. W.; Schenning, A. P. H. *J. Chem. Rev.* About Supramolecular Assemblies of π-Conjugated Systems. **2005**, 105 (4), 1491-1546.

(42)Coropceanu, V.; Cornil, J.; Filho, D. A. d. S.; Olivier, Y.; Silbey, R.; Brédas, J.-L. Charge Transport in Organic Semiconductors. Chem. Rev. 2007, 107, 926-952.

(43)Kim, H. U.; Kim, J. H.; Suh, H.; Kwak, J.; Kim, D.; Grimsdale, A. C.; Yoon, S. C.; Hwang, D-H. High open circuit voltage organic photovoltaic cells fabricated using 9,9′-bifluorenylidene as a non-fullerene type electron acceptor. *Chem. Commun*. **2013**, 49, 10950-10952.

(44)Biedermann, P. U.; Agranat, I. Stereochemistry of Bistricyclic Aromatic Enes and Related Polycyclic Systems. *Polyarenes II*. **2014**, 350, 177-277.

(45)Lee, J-S; Nyburg, S. C. Refinement of the a-Modification of 9,9'-Bifluorenylidene, C26H16, and Structure Analyses of the fl-Modification, the 2:1 Pyrene Complex, 2(C26H16).C16H10, and the 2:1 Perylene Complex, 2(C26H 16).C20 H 12. *Acta Cryst*. **1985**, C41, 560-567.

(46)Pogodin, S.; Rae, I. D.; Agranat, I. The Effects of Fluorine and Chlorine Substituents across the Fjords of Bifluorenylidenes: Overcrowding and Stereochemistry. *Eur. J. Org. Chem.* **2006**, 22.

(47)de la Harpe, C.; van Dorp, W. A. Ueber die Einwirkung des erhitzten Bleioxyds auf Fluoren. *Eur. J. Inorg. Chem*. **1875**, 8.

(48)Yeung, L. L.; Yip, Y. C.; Luh, T. –Y. W(CO)6-Mediated Desulfurdimerization of Dithioketals. Evidence for a Thione Intermediate. *J. Org. Chem*. **1990**, 55, 1874-1881.

(49)Lecher, H. Z.; Greenwood, R. A.; Whitehouse, K. C.; Chau, T. H. The Phosphonation of Aromatic Compounds with Phosphorus Pentasulfide. *J. Am. Chem. Soc*. **1956**, 78, 5018-5022.

(50)Cava, M. P.; Levinson, M. I. Thionation reactions of Lawesson's reagents. *Tetrahedron*. **1985**, 41, 5061-5087.

(51)Gaussian. http://gaussian.com/gaussview6/ (accessed Feb 15, 2017), Gaussview 6.

(52)Gaussian. http://gaussian.com/gaussian16/ (accessed Feb 15, 2017), Gaussvian 16.

(53)Gaussian. http://gaussian.com/people/?tabid=2 (accessed Feb 15, 2017), John Pople and Gaussian 70.

(54)Eckelmann, A. J. *My Life*, 1; Self: Springfield, MO, 2018.

(55)Gaussian. http://gaussian.com/keywords/ (accessed Feb 15, 2017), Keywords.

(56)Koch, W.; Holthausen, M. C. *A Chemist's Guide to Density Functional Theory*, 2; Wiley-VCH: Weinheim, Germany, 2001.

(57)W.; Sham, L. J. Self-Consistent Equations Including Exchange and Correlation Effects. *Phys. Rev.* **1965**, 140, A1133--A1138.

(58)Perdew, J. P.; Schmidt, K. In *Jacob's ladder of density functional approximations for the exchange-correlation energy* Proceedings of the AIP Conference. 2001, 577, 1–20.

(59)Yahweh. *Holy Bible*, King James; Church of England: London, England, 1611.

(60)Mardirossian, N.; Head-Gordon, M. ωB97X-V: A 10-parameter, range-separated hybrid, generalized gradient approximation density functional with nonlocal correlation, designed by a survival-of-the-fittest strategy. *Phys. Chem. Chem. Phys*., **2014**, 16, 9904-9924.

(61)Tao, J.; Perdew, J. P.; Staroverov, V. N.; Scuseria G. E.; Climbing the Density Functional Ladder: Nonempirical Meta–Generalized Gradient Approximation Designed for Molecules and Solids. *Phys. Rev. Lett*. **2003**, 91, 146401-4.

(62)Perdew, J. P.; Ernzerhof, M; Burke, K. Rationale for mixing exact exchange with density functional approximations. *J. Chem. Phys.* **1996**, 105, 9982–9985.

(63)Becke, A. D. A new mixing of Hartree–Fock and local density functional theories. *J. Chem. Phys*. **1993**, 98, 1372-1377.

(64)Kertész, M.; Koller, J; Ažman, A. Different orbitals for different spins for solids: Fully variational ab initio studies on hydrogen and carbon atomic chains, polyene, and poly(sulphur nitride). *Phys. Rev.* **1979,** B19, 2034-2040

(65)Young, D. Computational Chemistry. A Practical Guide for Applying Techniques to Real World Problems, 1; John Wiley & Sons. New York, NY, 2001.

(66)Dewar, M; Kirschner, S. Dimerization of Ethylene to Cyclobutane. *J. Am. Chem. Soc.* **1974**, 96, 5246-5247.

(67)Gilchrist, T. L.; Storr, R. C. *Organic Reactions and Orbital Symmetry*, 1; Cambridge University Press: Melborne, Australia, 1979.

(68)Sinnokrot, M. O.; Valeev, E. F.; Sherill, C. D. Estimates of the Ab Initio Limit for π−π Interactions: The Benzene Dimer. *J. Am. Chem. Soc.* **2002**, 124, pp 10887–10893.

(69)Rodriguez, A. M.; Prieto, P.; de la Hoz, A.; Diaz-Ortiz, A.; Martin, A.; Garcia, J. Influence of Polarity and Activation Energy in Microwave–Assisted Organic Synthesis (MAOS). *Chem. Op*. **2015**, 4, 308-317.

(70)Rakstys, K.; Saliba, M.; Gao, P.; Gratia, P.; Kamarauskas, E.; Paek, S.; Jankauskas, V.; Nazzeruddin, M. K. Highly Efficient Perovskite Solar Cells Employing an Easily Attainable Bifluorenylidene-Based Hole Transporting Material. Angew. *Chem. Int. Ed*. **2016**, 55, 7464-7468.

(71)Yu, T.; Guan, Guan, W.; Wang, X.; Zhao, Y.; Yang, Q.; Li, Yanmei, L.; Zhang, H. Synthesis and photophysical properties of 2,20-bis(oligothiophene)-9,90-bifluorenylidene derivatives. *New. J. Chem.* **2018**, 42, 2094-2103.

(72)Levy, A.; Goldschmidt, M. Agranat, I. A Simple Facile Synthesis of Bifluorenylidenes. *Lett. Org. Chem.* **2006**, 3, 579-584.

(73)Eliel, E.L.; Wilen, S.H.; Mander, L.N.*Stereochemistry of Organic Compounds*, Wiley, New York (1994).

(74)Stoyanov, E. S.; dos Passos Gomes, G. tert-Butyl Carbocation in Condensed Phases: Stabilization via Hyperconjugation, Polarization, and Hydrogen Bonding. *J. Phys. Chem*. **2015**, 119, 8619-8629.

(75)Pulay, P. A Perspective on the CASPT2 Method. *Int. J. Quantum Chem*. **2011**, 111, 3273–3279.